U.S. Department
of Transportation
National Highway
Traffic Safety
Administration

NHTSA

DOT HS 812 905 July 2020

Occupant Safety in Vehicles Equipped With Automated Driving Systems, Part 3: Biofidelity Evaluation of GHBMC M50-OS Against Laboratory Sled Tests

DISCLAIMER

Suggested APA Format Citation:

Poulard, D., Lin, H., & Panzer, M. B. (2020, July). *Occupant Safety in Vehicles Equipped With Automated Driving Systems, Part 3: Biofidelity Evaluation of GHBMC M50-OS Against Laboratory Sled Tests* (Report No. DOT HS 812 905). National Highway Traffic Safety Administration.

This report is one of three deliverables under Contract DTNH2215D00004/0002 awarded to the Center for Applied Biomechanics at the University of Virginia, Charlottesville, Virginia. The three are reports are titled as follows.

Occupant Safety in Vehicles Equipped With Automated Driving Systems, Part 1: Initial Evaluation of Usability, Stability, and Injury Prediction Capabilities

Occupant Safety in Vehicles Equipped With Automated Driving Systems, Part 2: Crash Safety Considerations for Out-of-Position Occupant Posture in Vehicles With Automated Driving Systems - Field Data Investigation

Occupant Safety in Vehicles Equipped With Automated Driving Systems, Part 3: Biofidelity Evaluation of GHBMC M50-OS Against Laboratory Sled Tests

The NHTSA citations and DOT HS report numbers for these three reports are as follows.

Lin, H., Gepner, B., Wu, T., Forman, J., Shaw, G., & Panzer, M. B. (2020, July). *Occupant safety in vehicles equipped with automated driving systems, Part 1: Initial evaluation of usability, stability, and injury prediction capabilities* (Report No. DOT HS 812 904). National Highway Traffic Safety Administration.

Shaw, G., Poplin, J., McMurry, T., Kong, K., Lin, H., & Panzer, M. B. (2020, February). *Occupant safety in vehicles equipped with automated driving systems, Part 2: Crash safety considerations for out-of-position occupant posture in vehicles with automated driving systems - Field data investigation* (Report No. DOT HS 812 883). National Highway Traffic Safety Administration.

Poulard, D., Lin, H., & Panzer, M. B. (2020, July). *Occupant safety in vehicles equipped with automated driving systems, Part 3: Biofidelity evaluation of GHBMC M50-OS against laboratory sled tests* (Report No. DOT HS 812 905). National Highway Traffic Safety Administration.

Technical Report Documentation Page

1. Report No. DOT HS 812 905	**2. Government Accession No.**	**3. Recipient's Catalog No.**
4. Title and Subtitle Occupant Safety in Vehicles Equipped With Automated Driving Systems, Part 3: Biofidelity Evaluation of GHBMC M50-OS Against Laboratory Sled Tests		**5. Report Date** July 2020 **6. Performing Organization Code**
7. Authors David Poulard, Hongnan Lin, Matthew B. Panzer		**8. Performing Organization Report No.**
9. Performing Organization Name and Address Center for Applied Biomechanics 4040 Lewis and Clark Drive Charlottesville, VA 22911		**10. Work Unit No. (TRAIS)** **11. Contract or Grant No.** DTNH2215D00004/0002
12. Sponsoring Agency Name and Address National Highway Traffic Safety Administration 1200 New Jersey Avenue SE Washington, DC 20590		**13. Type of Report and Period Covered** Final Report **14. Sponsoring Agency Code**
15. Supplementary Notes James Saunders was the COR for this project.		

16. Abstract

Current restraint systems and safety evaluation tools are based on a nearly 70-year developmental history, during which one primary factor remained consistent – the general position of the occupants. Automated Driving Systems (ADS) have an opportunity to disrupt this paradigm by allowing occupant positions not constrained by the need to actively control the vehicle. This report contains the summary report assessing the validity of the responses of the Global Human Body Models Consortium (GHBMC) male 50th percentile occupant (M50-O), Global Human Body Models Consortium (GHBMC) male 50th percentile simplified occupant (M50-OS), and the test device for human occupant restraint – finite element (THOR FE) models against available 30 km/h, 30° sled test, referenced in this report as GS3, each using a postmortem human subject (PMHS).

17. Key Words		**18. Distribution Statement** Document is available to the public from the National Technical Information Service, www.ntis.gov.	
19. Security Classif. (of this report) Unclassified	**20. Security Classif. (of this page)** Unclassified	**21. No. of Pages** 73	**22. Price**

Form DOT F 1700.7 (8-72) **Reproduction of completed page authorized**

Contents

Executive Summary

Current restraint systems and safety evaluation tools are based on a nearly 70-year developmental history during which one primary factor remained consistent – the general position of the occupants. Automated Driving Systems (ADS) have an opportunity to disrupt this paradigm by allowing occupant positions not constrained by the need to actively control the vehicle.

This deliverable contains the summary report assessing the validity of the responses of the Global Human Body Models Consortium (GHBMC) male 50th percentile occupant (M50-O), Global Human Body Models Consortium (GHBMC) male 50th percentile simplified occupant (M50-OS), and the Test Device for Human Occupant Restraint – Finite Element (THOR FE) models against available 30 km/h, 30° sled test, referenced in this report as GS3, each using a postmortem human subject (PMHS).

1 Material and Methods

1.1 Overview of the experiments

The Gold Standard 3 (GS3) test is a 30 km/h, 30° near-side oblique frontal impact sled test using a custom 3 kN force-limited shoulder-belt and a seat modified from the original Gold Standard sled setup (Figure 1). This sled test configuration is consistent with a frontal crash scenario with the seat oriented in-board, and it is a configuration likely to be considered for the Automated Driving System Evaluation Plan.

In this study, we are using the experimental data from three male PMHSs, similar in mass and size to a 50th percentile male, and 4 tests conducted with the THOR anthropomorphic test dummy (ATD) in GS3 (Table 1)

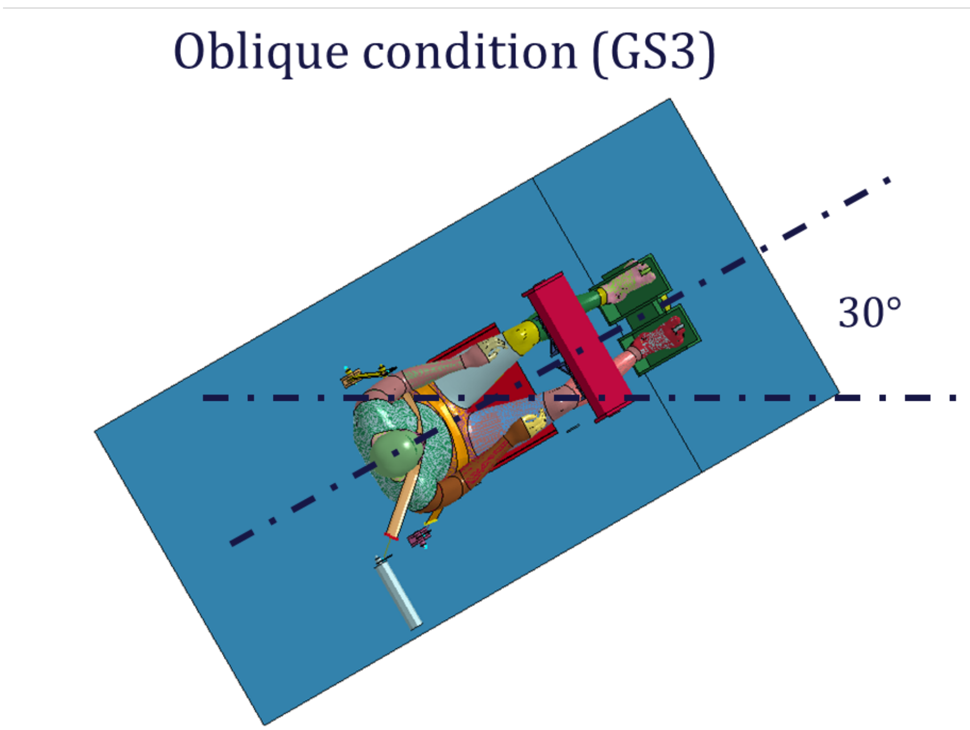

Figure 1. Gold Standard 3 sled configuration

Table 1. Test Matrix.

Test Condition	Surrogates	Test Number
GS3 Gold Standard Condition 3 30 km/h, 3 kN Force-Limited Belt	PMHS	S0313
	PMHS	S0314
	PMHS	S0315
	THOR	S0309
	THOR	S0310
	THOR	S0311
	THOR	S0312

In each of these tests, PMHSs and THOR were equipped with standard instrumentation in addition to a high-speed three-dimensional (3D) motion capture system (Vicon MX) that was used to quantify occupant kinematics and restraint interactions (Figure 2). In the PMHS, Vicon markers were surgically-implanted using multi-marker arrays to facilitate 3D tracking of select individual skeletal structure (the skull, individual vertebrae, etc.; Shaw et al., 2009, Lessley et al., 2011). Injuries were documented post-test via computerized tomography (CT) scan and autopsy of the PMHS.

Torso motion and chest deflection were the primary responses recorded for both PMHSs and THOR.

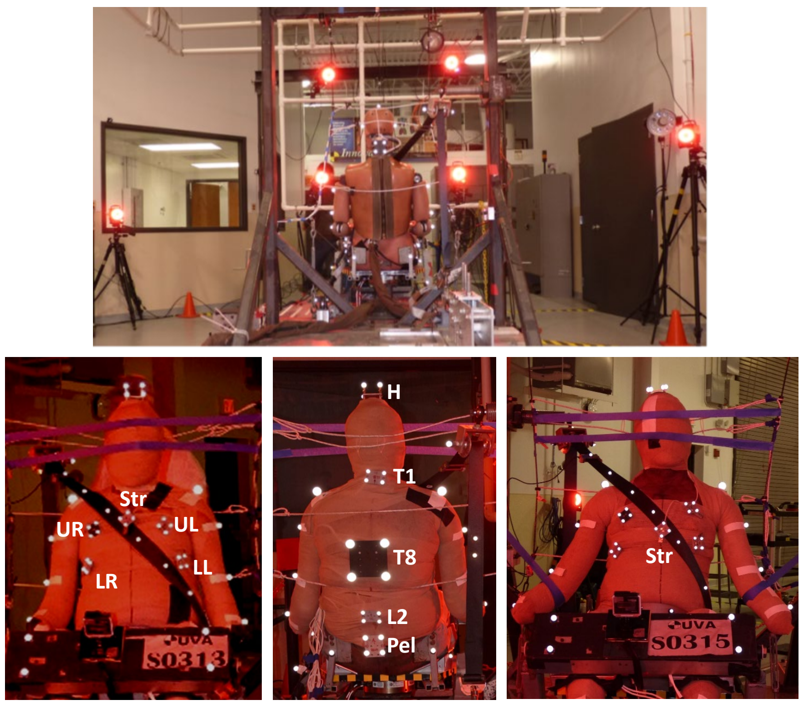

Figure 2. Detailed 3-D motion tracking by VICON

1.2 Environment model

We adapted the existing Gold Standard buck finite element (FE) model (developed by the UVA-CAB) to replicate the GS3 test environment (Figure 3). In this model, a number of key components were modeled as rigid bodies (base plate, seat plate, back support plate, D-ring, outboard anchor, inboard anchor, rod, buckle, foot plate, and knee bolster). The load cells in the foot plate, knee bolster, and seat plate were replicated using beam elements that can measure the six degree-of-freedom reaction forces and moments (Fx, Fy, Fz, Mx, My, and Mz).

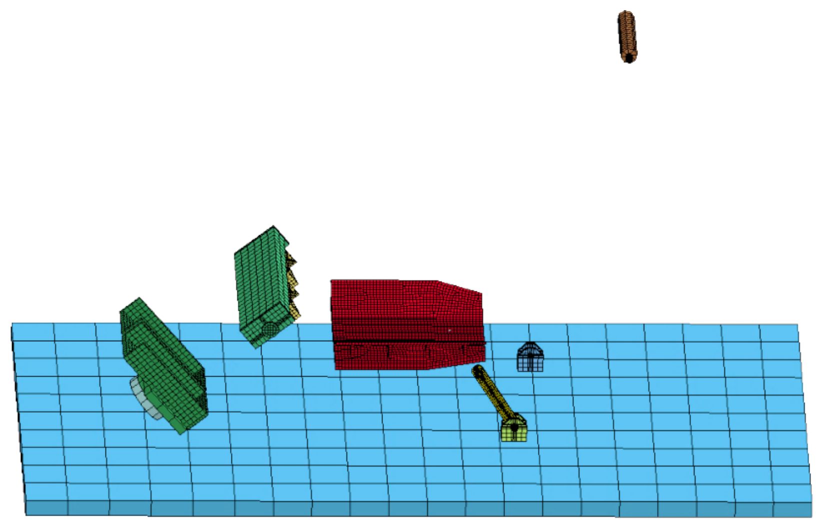

Figure 3. Modified GS3 Buck.

The modifications to the Gold Standard buck FE model needed to replicate the GS3 sled environment include:

- Modified the seat that was designed to prevent lateral pelvic motion (Figure 4); and
- Updated restraint anchor locations on the buck according to the experimental location (Figure 5).

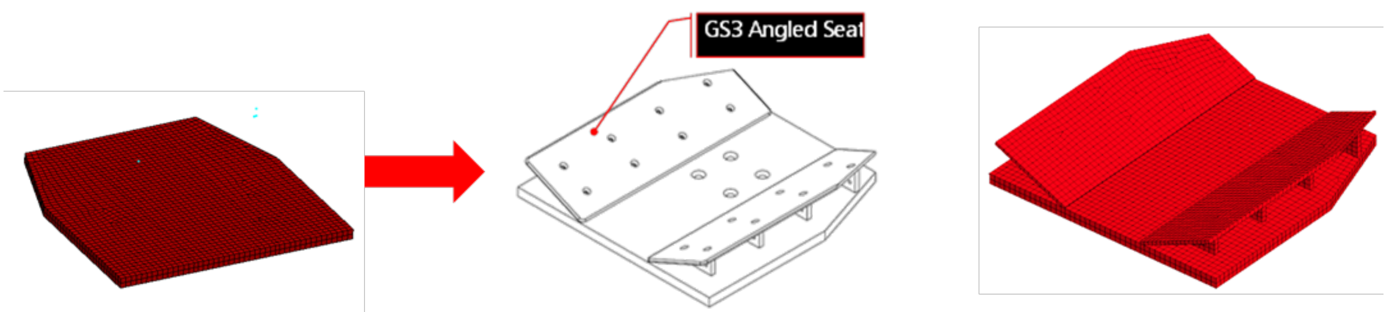

Figure 4. CAD and FE GS3 angle seat.

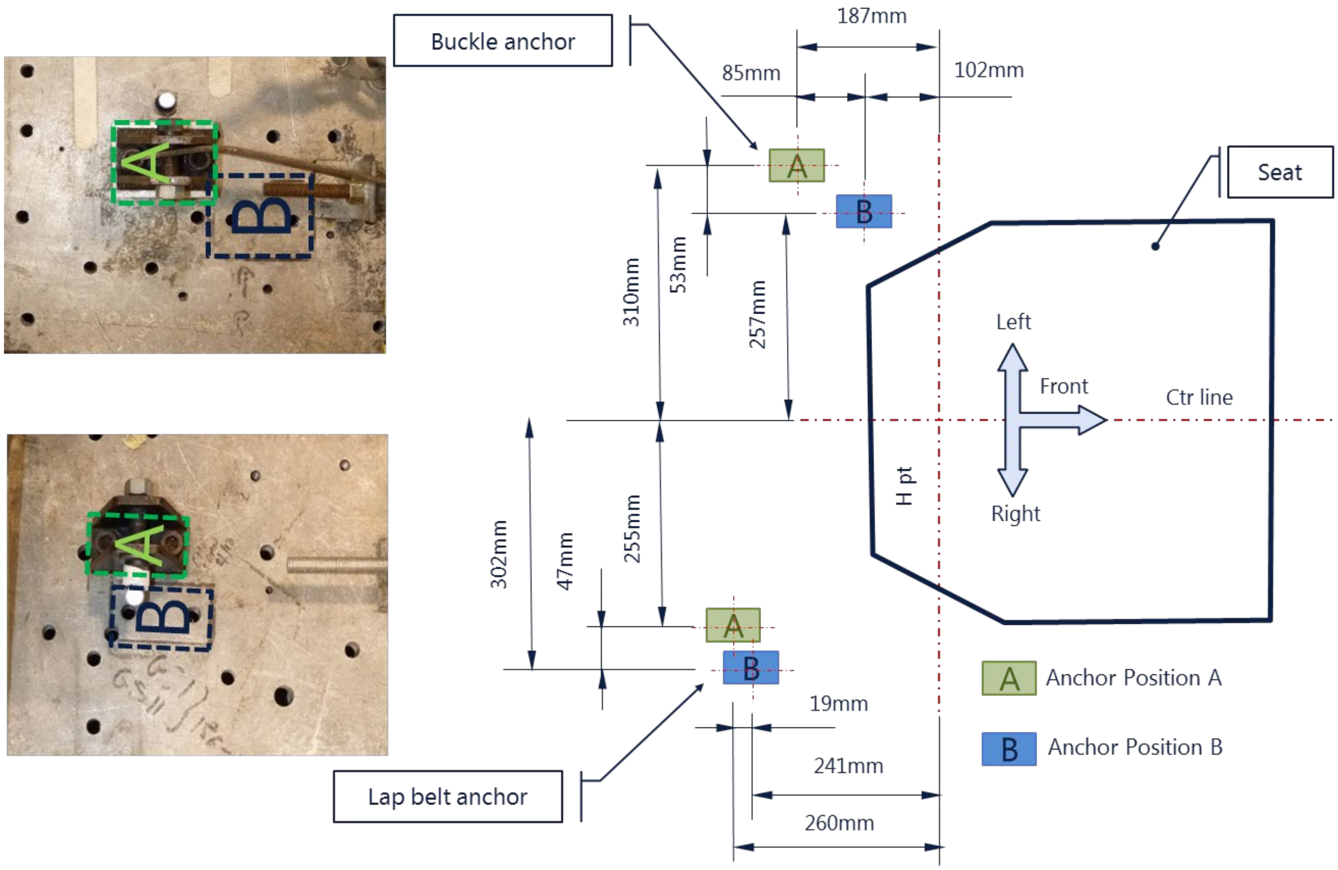

Figure 5. Restraint anchors on the buck.

The models were subjected to a prescribed deceleration based on the average trapezoidal pulse obtained in the experiments (Shaw et al., 2009) (Figure 6).

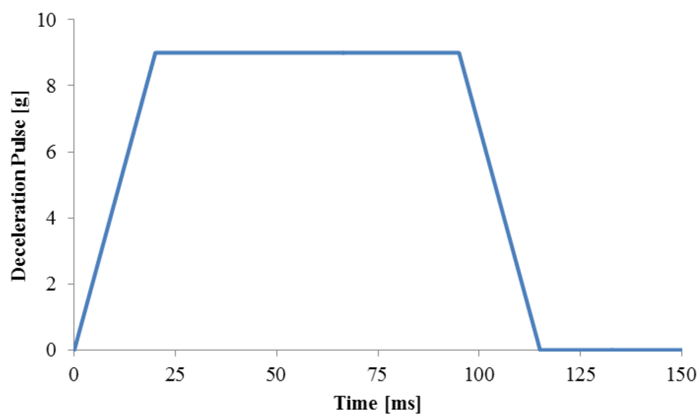

Figure 6. Prescribed deceleration pulse.

1.3 Positioning

The occupant position measurements taken during the GS3 tests were gathered in Table 2 for PMHSs and in Table 3 for THOR. Based on the averaged values for all of the tests, positioning goals were determined for the human body models (HBM) and THOR FE and are identified as *Target* in the respective tables.

Table 2. PMHS Positioning Parameters.

	A	B	C	D	E
	Right Hpt Distance (relative to the target)	Torso Angle	Sternal Angle	Femur Angle (Right)	Tibia Angle (Right)
Test #	**mm**	**deg.**	**deg.**	**deg.**	**deg.**
S0313	-13	9	31	13	42
S0314	-14	7	20	5	42
S0315	-15	9	14	11	39
Target	0	8.3	22	10	41
M50-OS	0	8.2	24	7	39
M50-O	0	8.2	24	7	39

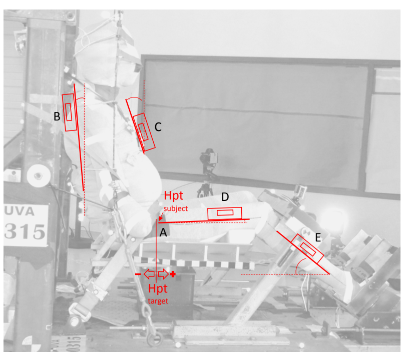

Measurements Definition

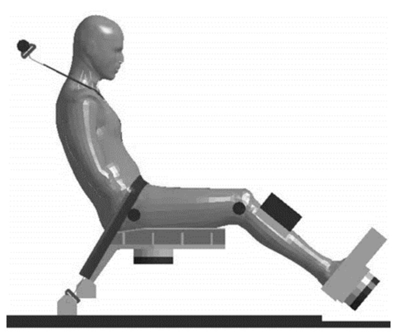

GHBMC M50-OS

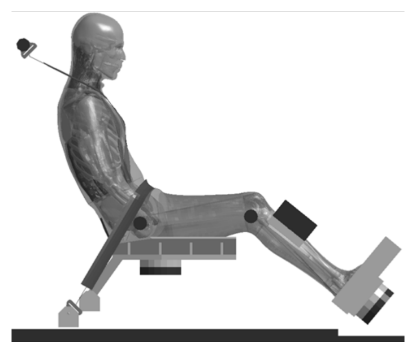

GHBMC M50-O

Table 3. THOR Positioning Parameters.

	A	B	C	D
	Right Hpt Distance (relative to the target)	Lower Spine Angle	Femur Angle (Right)	Tibia Angle (Right)
Test #	mm	deg.	deg.	deg.
S0309	2	86.3	3.2	32.8
S0310	5	N/A	2.9	33.1
S0311	4	86.5	3.2	33.5
S0312	3	86.5	3.1	33.5
Target	0	86.4	3.0	33.2
THOR-FE	0	86.4	3.0	33.2

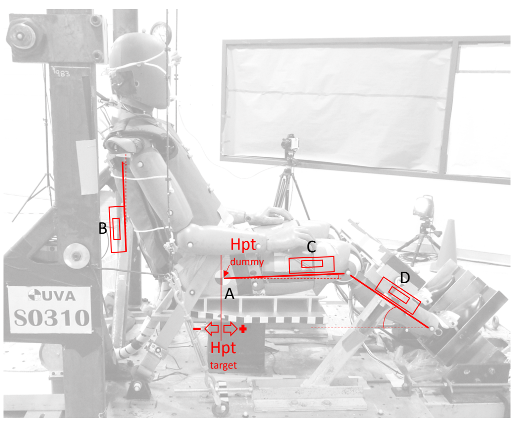

Measurements Definition

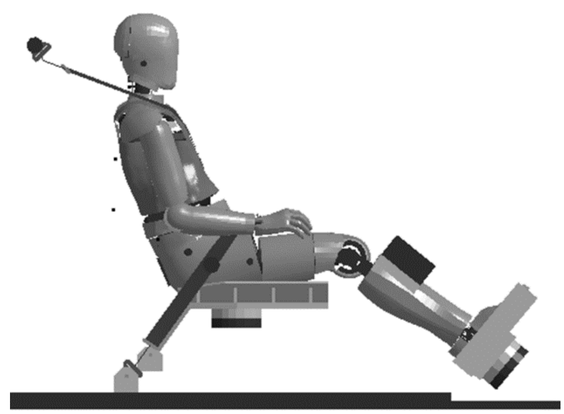

THOR FE

To do so, the positioning trees defined in GHBMC-M50-OS for their limbs were used (Figure 7). For the GHBMC M50-O, a step-by-step computational framework was developed (Figure 8). For the HBM, arms were cut off as in experiments.

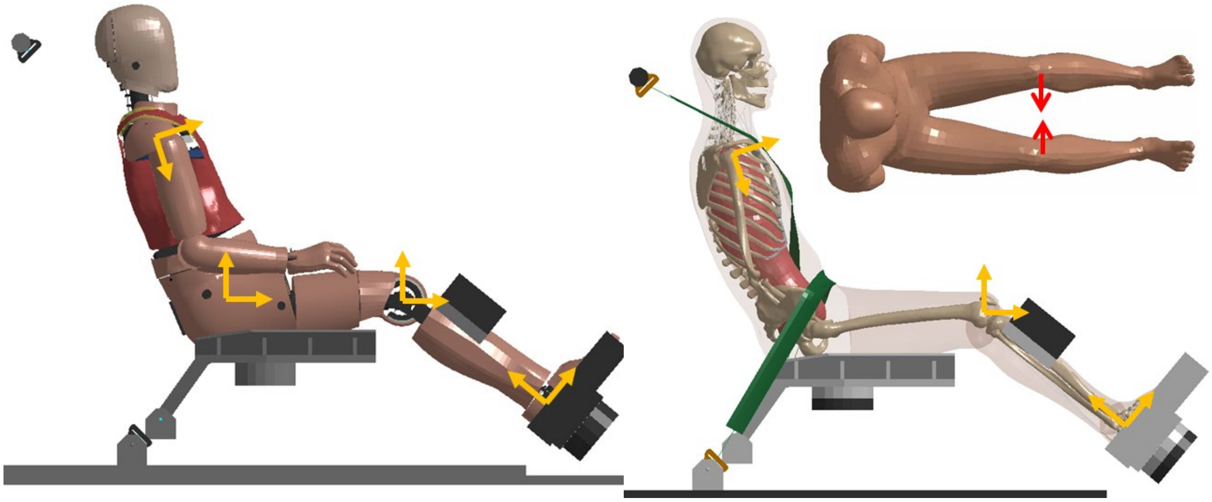

Figure 7. Pre-defined positioned tree in THOR v2.2 and GHBMC M50-OS.

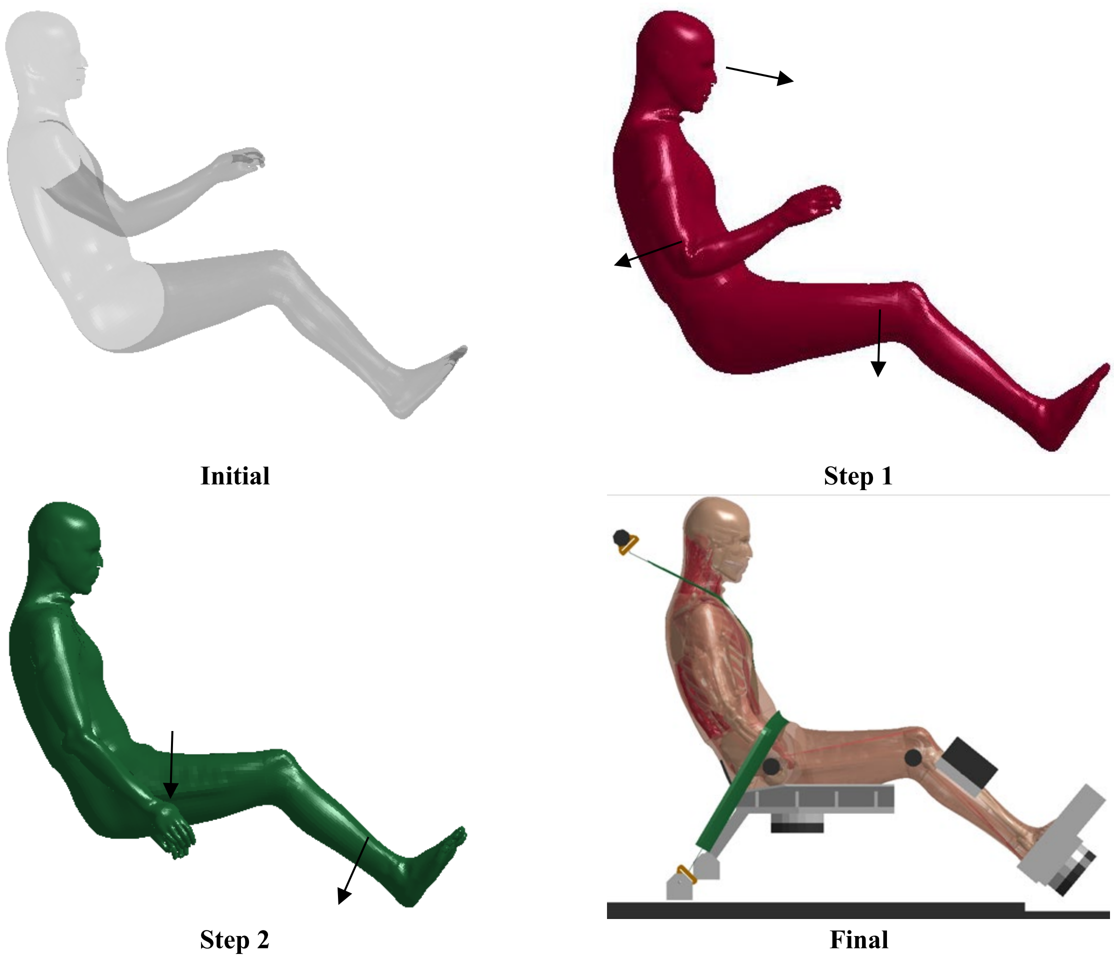

Figure 8. Step-by-step computational framework to position GHBMC M50-O.

The settlement was performed without any pre-simulation by adding penetration with the seat in conjunction with the “seat deformer” tool included in LS-Prepost (Figure 9), which computed stress from the deformation gradient matrix.

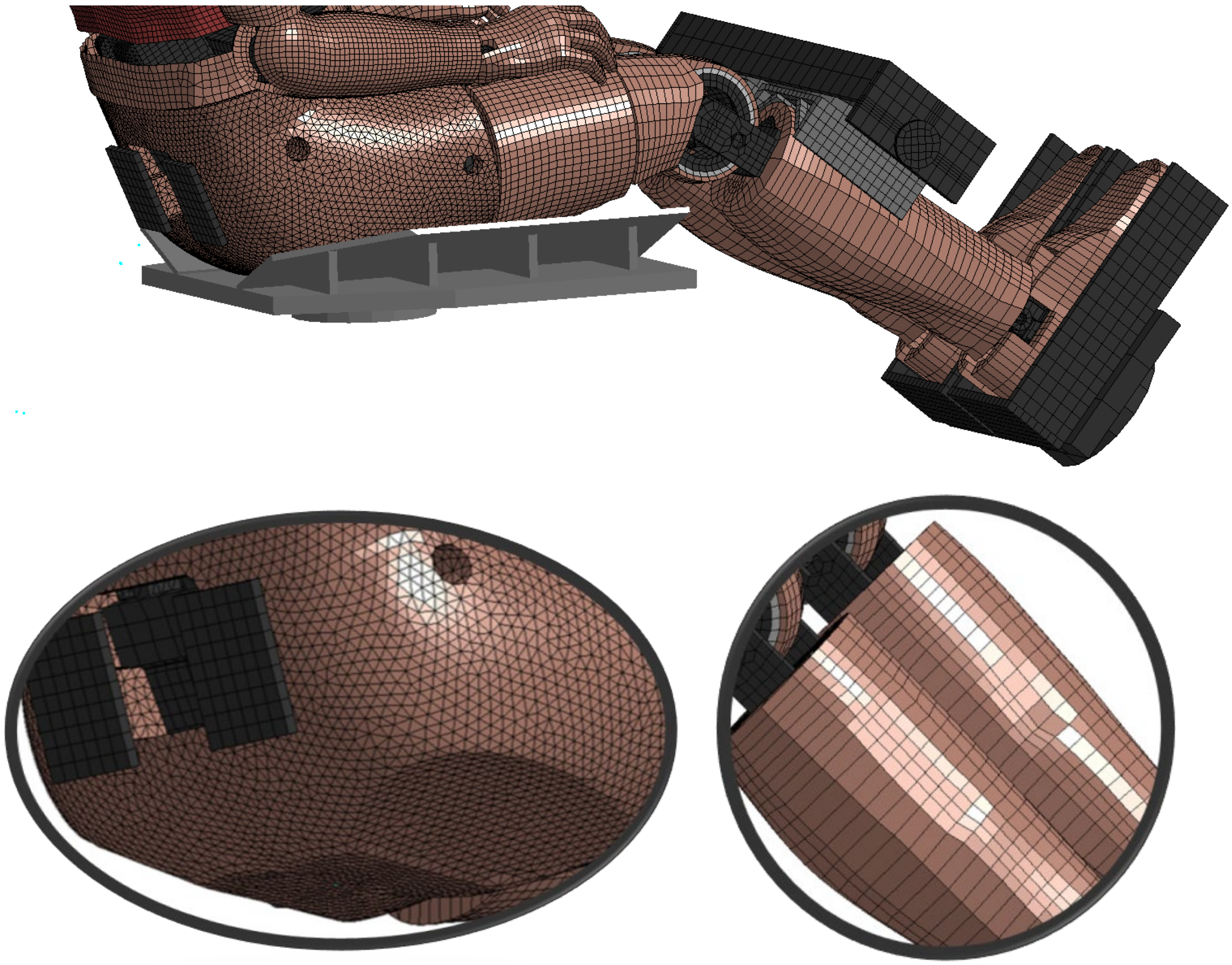

Figure 9. Settling using the seat deformer tool included in LS-Prepost

1.4 Belt modeling

By default, the belt should cross the thorax at the midsternum and midclavicle, as it was intended to be in the experiments. Variability in belt paths was observed in the experiments so the belt measurement taken during the GS3 tests were gathered in Table 4 for PMHSs and in Table 5 for THOR. Based on the averaged values for all of the tests, positioning goals were determined for the HBM and THOR FE and are identified as *Target* in the respective tables.

To facilitate the process the BeltFit tool from LS-PrePost was used. The shoulder as well as the lap belt were created using the mixed technique, where seat belt (1D) elements were used close to the attachment points (D-ring and anchor points) and shell tria (2D) elements were used for the remaining section of the belt to ensure proper interaction between the belt and the human body. The belts were stretched one time with the use of the BeltFit "STRETCH" function to better fit to the model geometry. The friction coefficient between the belts and the body was set to 0.5. The material properties for the belts were based on Shaw et al., 2009.

Table 4. PMHS Belt Parameters.

	A	B	C	D
	Outer belt edge to acromion lateral border	Sternal notch to upper belt edge	Angle of upper belt edge at midline (from frontal photo)	Angle of upper belt edge of shoulder (from lateral photo)
Test #	**mm**	**mm**	**deg.**	**deg.**
S0313	51	48	46	32
S0314	51	48	45	29
S0315	45	70	47	31
Target	49	55	46	31
M50-OS	49	50	47	30
M50-O	49	50	47	30

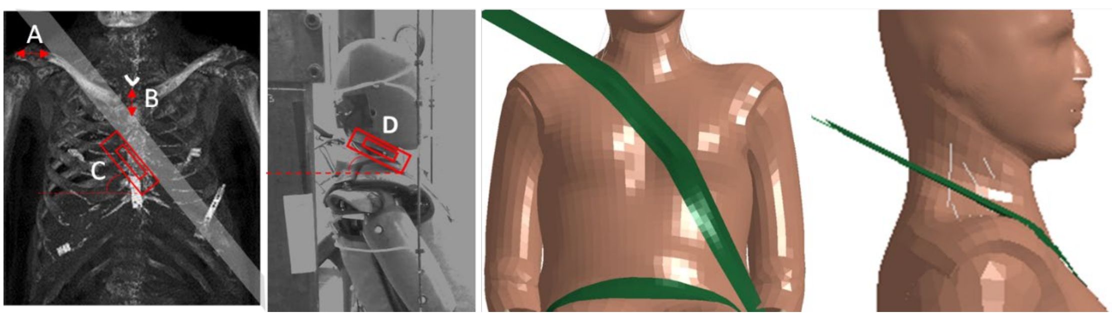

Table 5. THOR Belt Parameters.

	B	C	D	E
	Chin to medial belt edge at centerline	Angle of upper edge of belt with level on centerline relative to horizontal	Plate on proximal thighs to bottom edge of belt on centerline	Angle of belt as it leaves shoulder relative to horizontal in the plane of the belt
Test #	**mm**	**deg.**	**mm**	**deg.**
S0309	112	49.1	294	26.5
S0310	113	50.4	294	24.3
S0311	115	50.1	295	24.7
S0312	105	49.6	302	24.8
Target	111 ± 4.3	49.8 ± 0.6	296 ± 3.9	25.1 ± 1.0
THOR FE	111	50.0	296	25.0

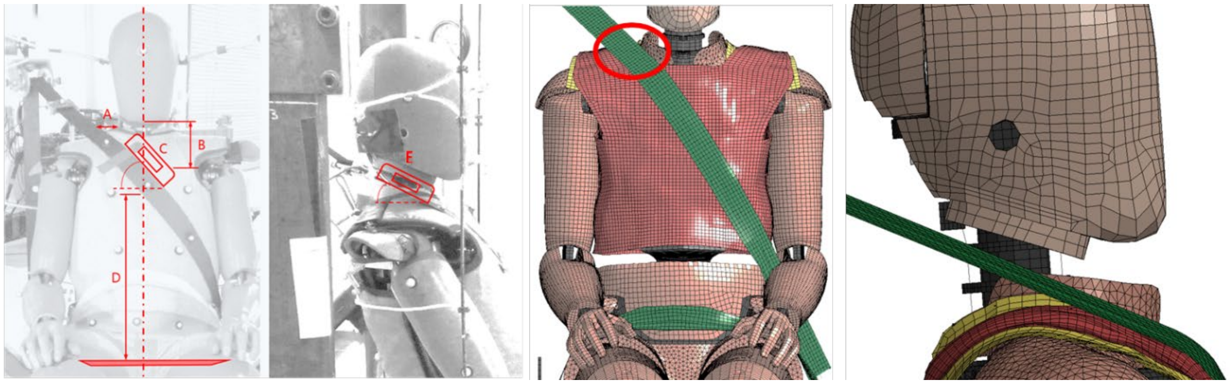

The belt characteristics provided by the manufacturer were discretized and used in the seat belt material definition (6-8% elongation, 10.7 kN tensile strength). The belt load path was defined using the LS-Prepost Seat belt Fitting tool. In the modeling approach, the seat belt is composed of both 2D and 1D seat belt elements (Figure 10). The 2-D elements are shells with a fully integrated membrane formulation spread on the occupant torso for a better contact during impact. The force limiting mechanism was modeled by using 1D elastoplastic seat belt element, with a yield force in the belt was equal to the experimental force limit (2.7 kN)

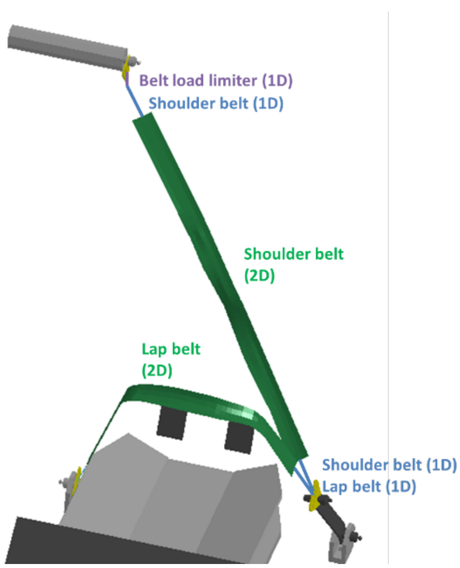

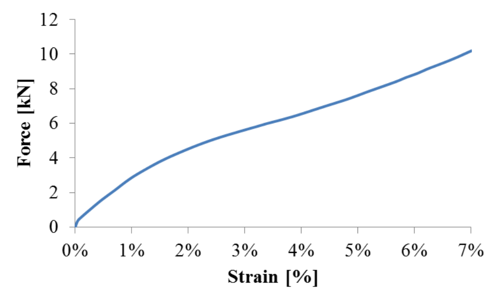

Belt load curve

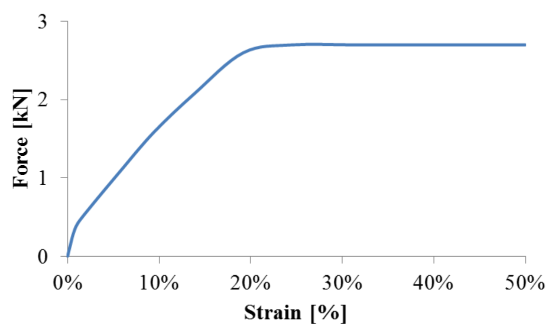

Belt limiter load curve

Figure 10. Belt Modeling

1.5 Model instrumentation

Models and markers of the sensors used in GS3 (acceleration cubes, Vicon markers, etc.) were added to the HBM to compare with the PMHS response and FE model output. The sensor model package was incorporated to the original model files. THOR FE already contained a majority of the instrumentation measurement points and only Vicon markers were added.

3D displacements of the head, the spine (T1, T8, L2, and L4), and the pelvis relative to the vehicle coordinate system were measured from the model. The anatomical centers were defined according to Wu et al. (2005) (Figure 11).

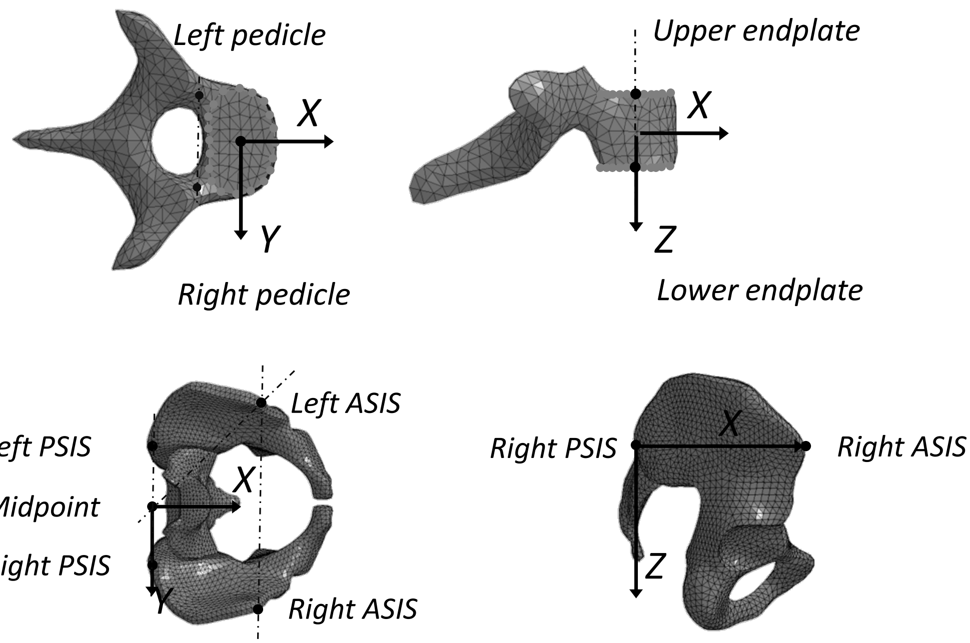

Figure 11. Anatomical coordinates systems

1.6 Quantitative assessment of the response of the model

A quantitative assessment of the response of the models compared to the experiments was performed through metrics obtained with the CORA software (CORelation and Analysis, Partnership for Dummy Technology and Biomechanics) (Gehre et al., 2009). Each of these metrics, including the corridor, the phase, the magnitude and the slope, is given a sub-score and the weighed sum of these sub-scores is the CORA score ranging between 0 and 1. The weighting factors of the sub-scores are 0.4 for the corridor, 0.2 for the phase, 0.2 for the magnitude and 0.2 for the slope.

1.7 Injury assessment

Unlike its more detailed counterpart, the GHBMC M50-OS is not intended to predict crash induced injuries based on tissue-level criterion, but virtual instrumentation such as accelerometers or deflection sensors that we evaluated are meant to be the proxy.

M50-O was initially designed to computationally predict common fractures (rib, clavicle) using a deterministic method, inferred when a cluster of elements representing a bone are deleted (eroded). However, in this study, we disabled element deletion to improve stability. Consequently, bone fracture risk has been assessed through post-processing using two different methods.

1. **Deterministic**: clavicle, sternum and cervical fractures were defined via post-processing when the effective plastic strain reached the value defined for the model (1.78%).
2. **Probabilistic**: the risk of rib fracture was defined using a strain-based injury risk function that could account for tolerance variations in the population (Forman et al., 2012).

2 Results

2.1 GHBMC M50-OS and GHBMC M50-O

Model Stability Assessment

No model instability was reported during the simulation for M50-OS. Simulation runs in 90 minutes on a 24-CPUs cluster.

Partial remeshing of the M50-O pelvis flesh was necessary to eliminate elements with poor mesh quality caused by the positioning process.

The timestep was reduced by 30 percent for M50-O to ensure the model stability up to 250 ms. Simulation ran in 49 hours on a 24-CPUs cluster.

Shoulder Belt Loads

Upper shoulder belt time histories are provided in Figure 12.

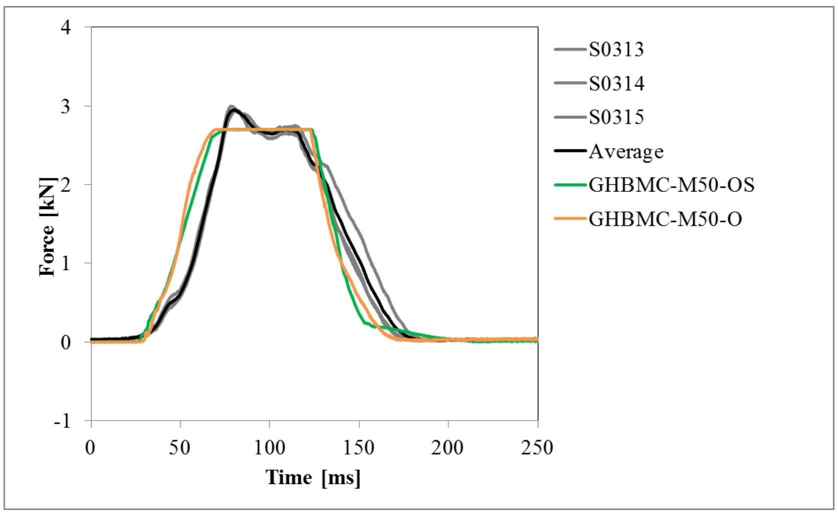

Figure 12. Upper shoulder belt loads comparison of M50-OS and M50-O simulation data with PMHS sled tests.

Occupant Kinematics

Motions of the head, spine, shoulders, and pelvis are provided in Figure 13 to Figure 21 relative to the sled buck. Peak excursion values for all measurements locations in the X, Y, and Z-axis directions are provided in Table 6.

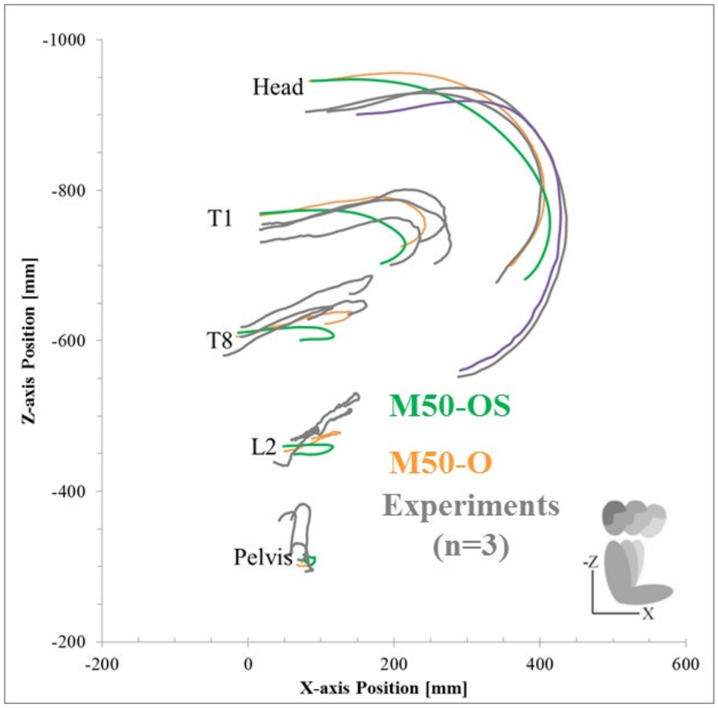

Figure 13. Spine trajectory for M50-OS and M50-O relative to PMHS response (lateral view)

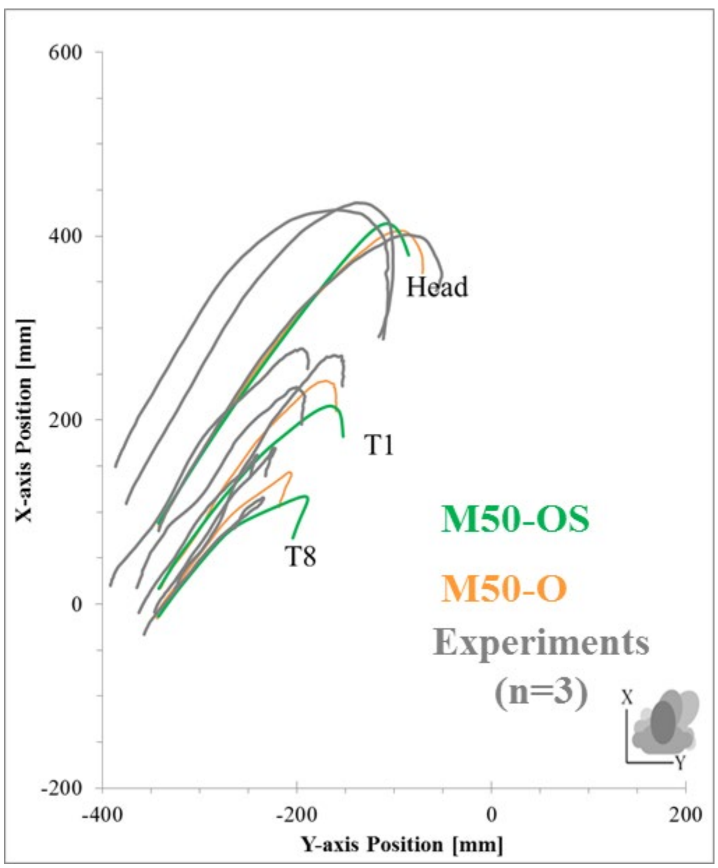

Figure 14. Spine trajectory for M50-OS and M50-O relative to PMHS response (top view)

Table 6. Peak excursions between 0-175ms for PMHS, M50-OS, and M50-O.

		X		Y		Z	
		Min	Max	Min	Max	Min	Max
Head	S0313	0	322	0	291	-25	239
	S0314	0	279	0	280	-18	344
	S0315	0	327	0	274	-31	359
	average	**0**	**309**	**0**	**282**	**-25**	**314**
	st dev	**0**	**26**	**0**	**9**	**7**	**65**
	M50-OS	0	326	0	284	-2	267
	M50-O	0	322	0	271	-10	255
L Shoulder	S0313	0	336	0	262	-89	0
	S0314	0	333	0	279	-76	0
	S0315	0	353	0	296	-103	0
	average	**0**	**341**	**0**	**279**	**-89**	**0**
	st dev	**0**	**10**	**0**	**17**	**14**	**0**
	M50-OS	*0*	*212*	*0*	*209*	*-20*	*0*
	M50-O	*-9*	*116*	*0*	*195*	*-12*	*9*
R Shoulder	S0313	0	220	0	132	-37	8
	S0314	0	225	0	129	-38	11
	S0315	0	224	0	136	-33	19
	average	**0**	**223**	**0**	**132**	**-36**	**13**
	st dev	**0**	**3**	**0**	**4**	**3**	**6**
	M50-OS	*0*	*184*	*0*	*182*	*-2*	*73*
	M50-O	*0*	*158*	*0*	*104*	*-10*	*45*
T1	S0313	0	254	0	173	-53	18
	S0314	0	218	0	173	-32	33
	S0315	0	258	0	294	-32	56
	average	**0**	**243**	**0**	**183**	**-39**	**36**
	st dev	**0**	**22**	**0**	**18**	**12**	**19**
	M50-OS	*0*	*198*	*0*	*196*	*-5*	*72*
	M50-O	*0*	*226*	*0*	*182*	*-12*	*48*
T8	S0313	0	179	0	124	-68	0
	S0314	0	149	0	123	-64	0
	S0315	0	172	0	122	-48	0
	average	**0**	**166**	**0**	**123**	**-60**	**0**
	st dev	**0**	**16**	**0**	**1**	**11**	**0**
	M50-OS	*0*	*130*	*0*	*153*	*-7*	*23*
	M50-O	*0*	*112*	*-1*	*152*	*-10*	*1*
L2	S0313	0	91	0	85	-61	1
	S0314	0	61	-3	60	-45	5
	S0315	0	82	0	68	-41	0
	average	**0**	**78**	**-1**	**71**	**-49**	**2**
	st dev	**0**	**15**	**2**	**13**	**11**	**3**
	M50-OS	*-19*	*68*	*0*	*122*	*-2*	*18*
	M50-O	*-5*	*77*	*0*	*103*	*-26*	*0*
Pelvis	S0313	-10	16	0	56	-74	1
	S0314	-19	10	0	41	-38	0
	S0315	-8	16	0	36	-59	0
	average	**-12**	**14**	**0**	**45**	**-57**	**0**
	st dev	**6**	**3**	**0**	**10**	**18**	**0**
	M50-OS	*-7*	*13*	*0*	*77*	*-11*	*4*
	M50-O	*-10*	*14*	*0*	*67*	*-24*	*5*

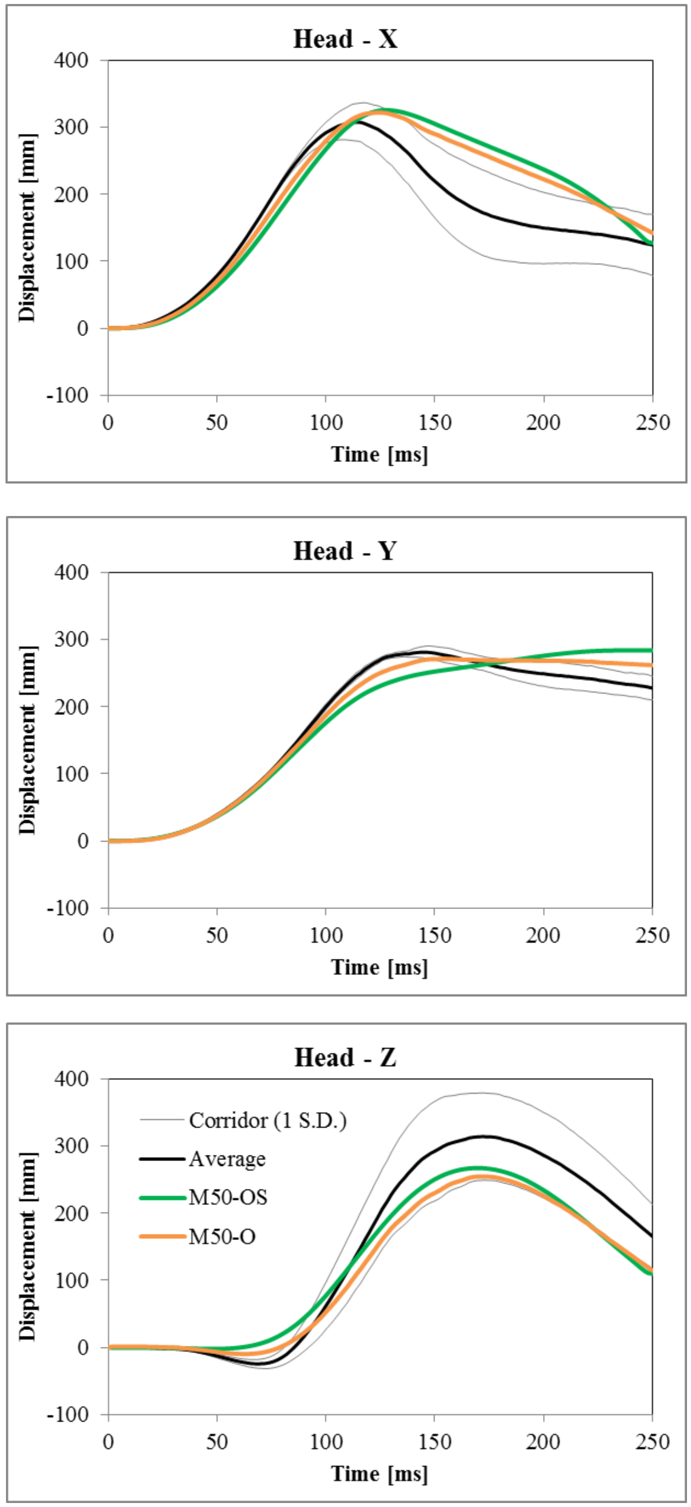

Figure 15. Displacements of the M50-OS and M50-O head relative to the buck, compared to PMHS results.

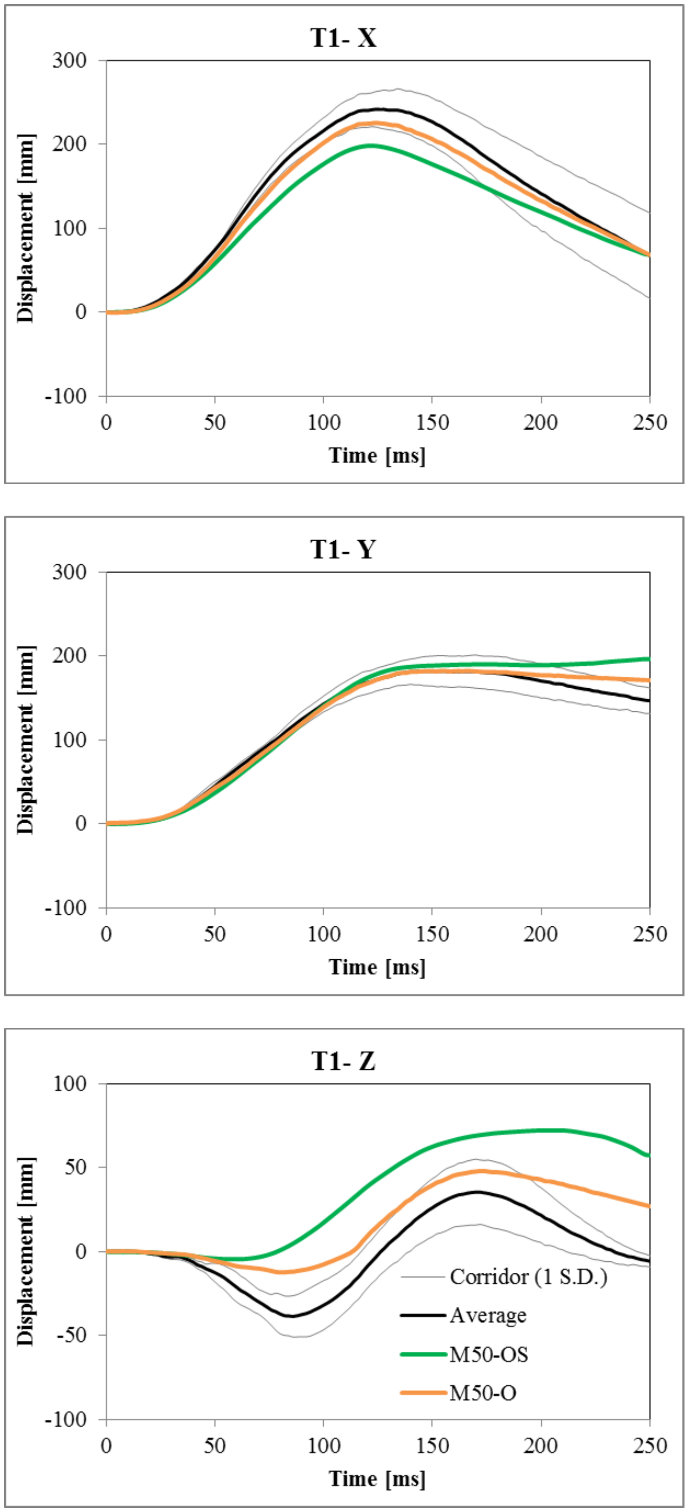

Figure 16. Displacements of the M50-OS and M50-O T1 relative to the buck, compared to PMHS results.

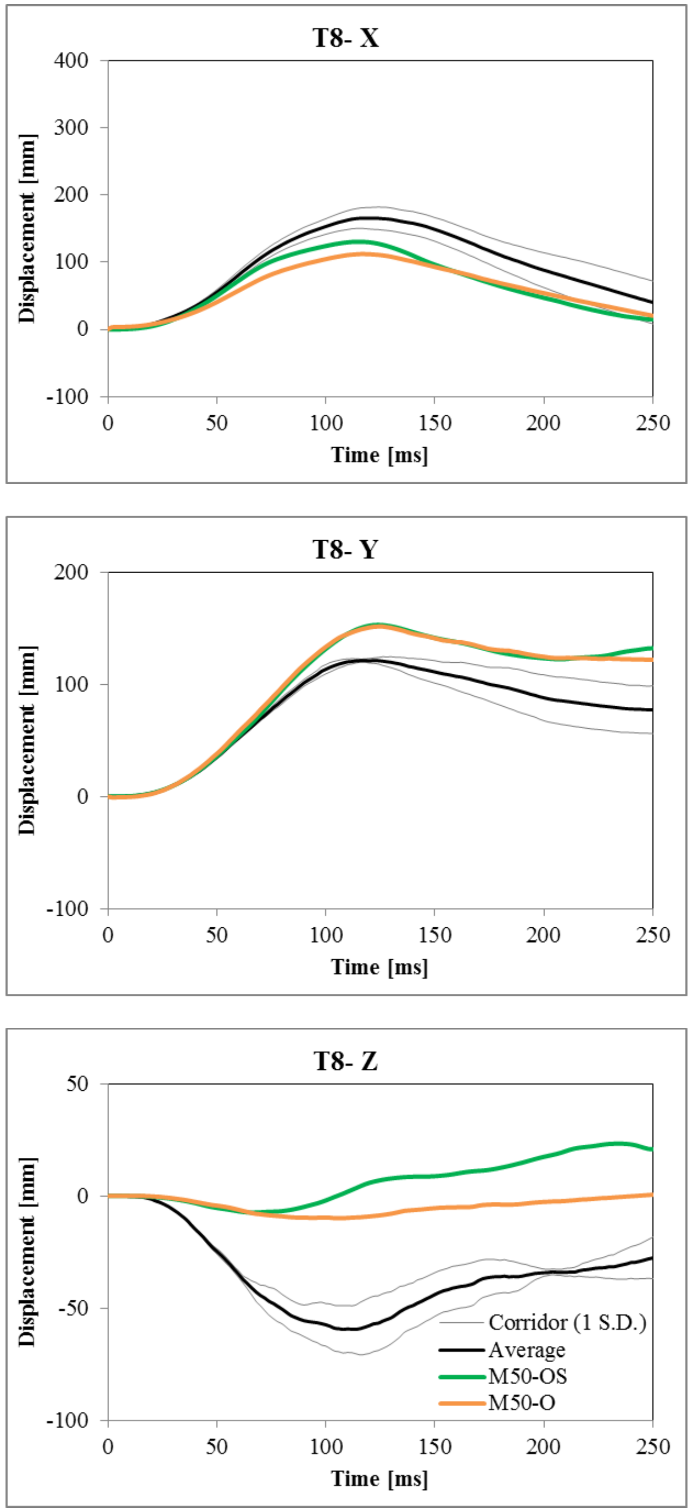

Figure 17. Displacements of the M50-OS and M50-O T8 relative to the buck, compared to PMHS results.

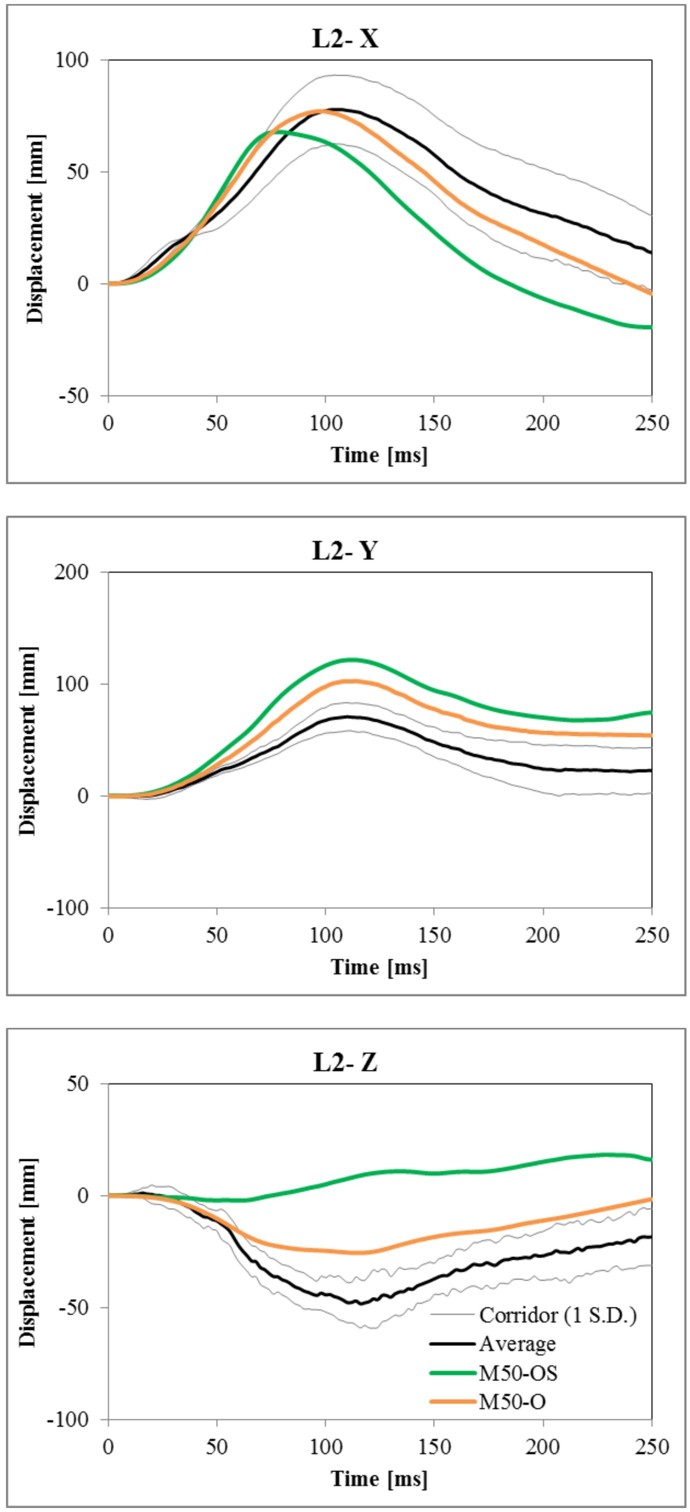

Figure 18. Displacements of the M50-OS and M50-O L2 relative to the buck, compared to PMHS results.

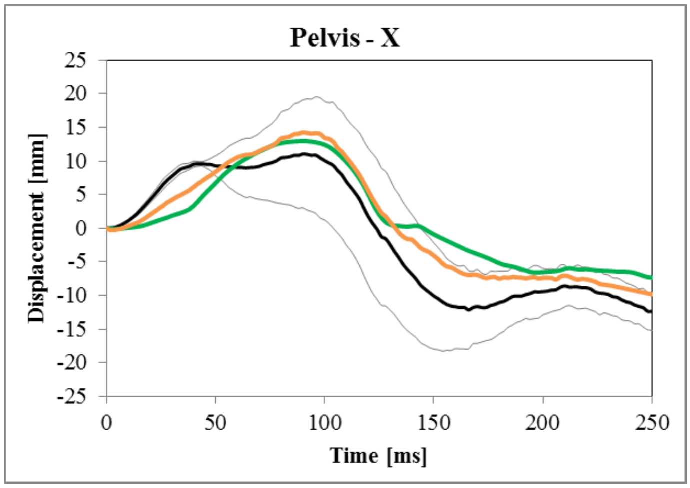

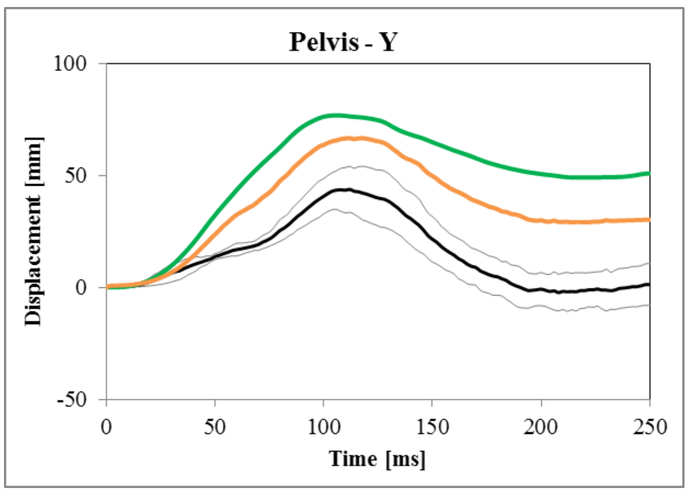

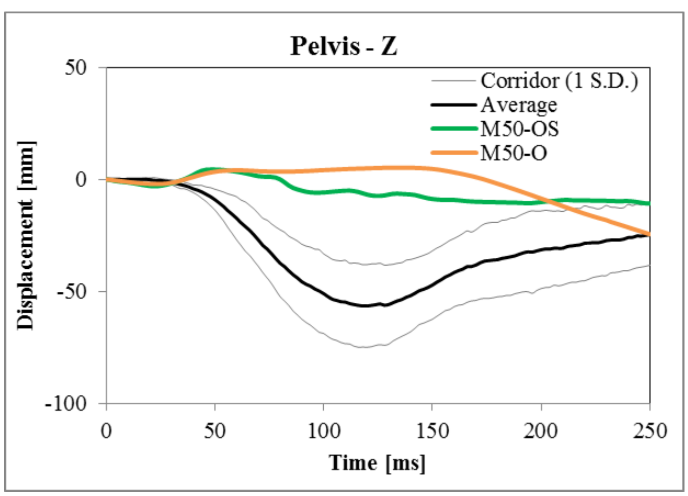

Figure 19. Displacements of the M50-OS and M50-O pelvis relative to the buck, compared to PMHS results.

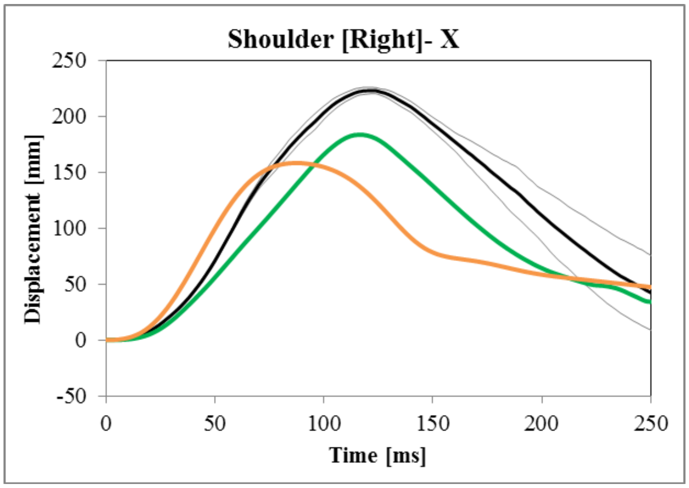

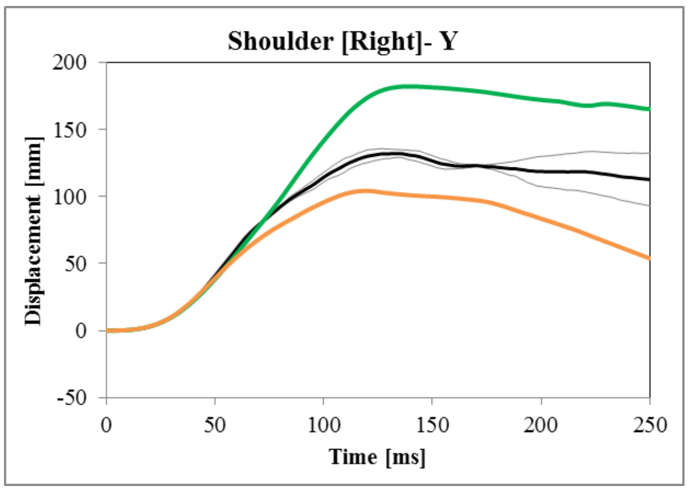

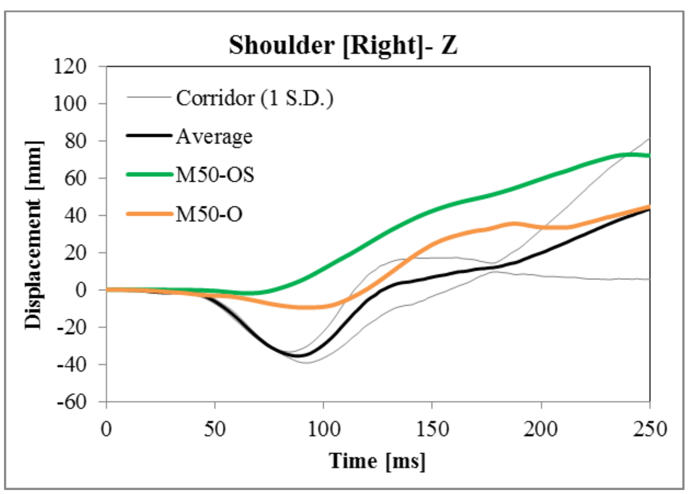

Figure 20. Displacements of the M50-OS and M50-O right shoulder relative to the buck, compared to PMHS results.

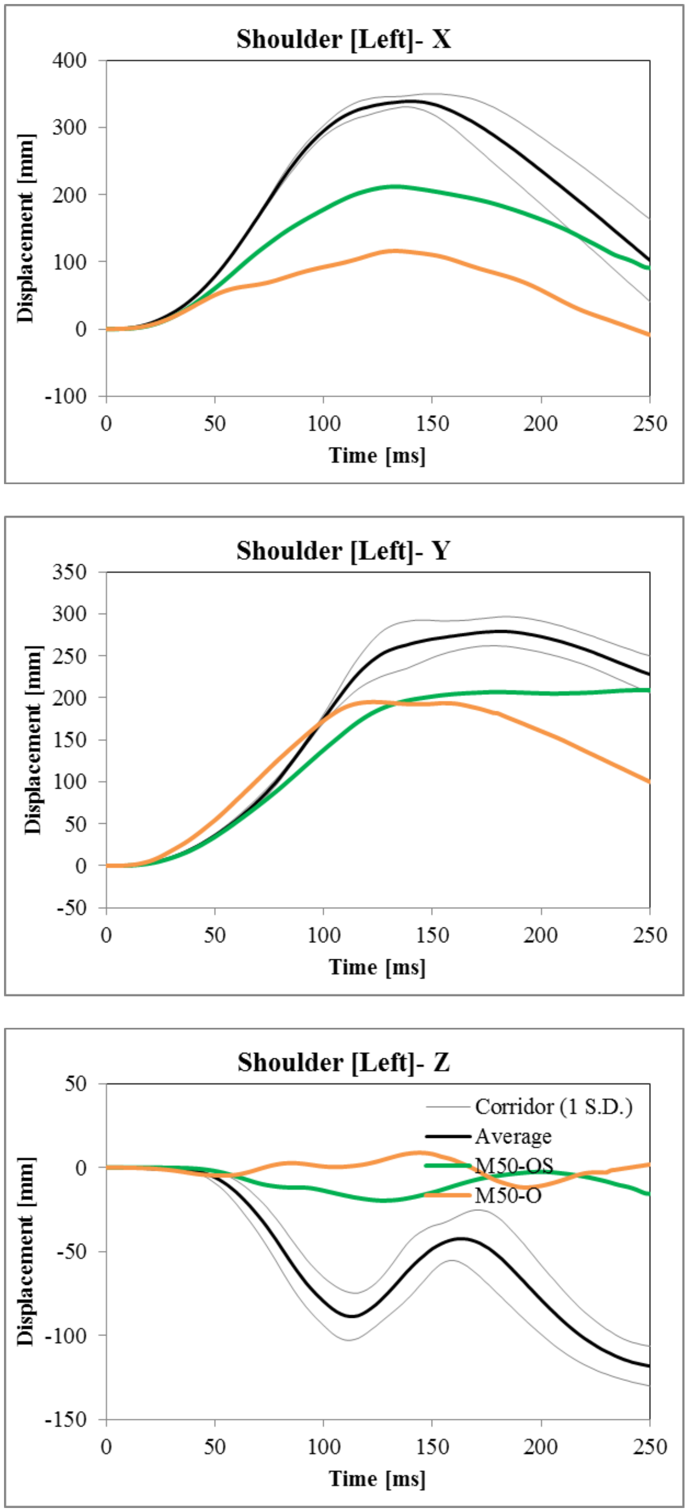

Figure 21. Displacements of the M50-OS and M50-O left shoulder relative to the buck, compared to PMHS results.

Chest Deflection

Processed Infra-Red Telescoping Rod for the Assessment of Chest Compression (IR-TRACC) deflection time-history plots are provided from Figure 22 to Figure 25. Average peak IR-TRACC X, Y, and Z-axis deflection values are presented in Table 7.

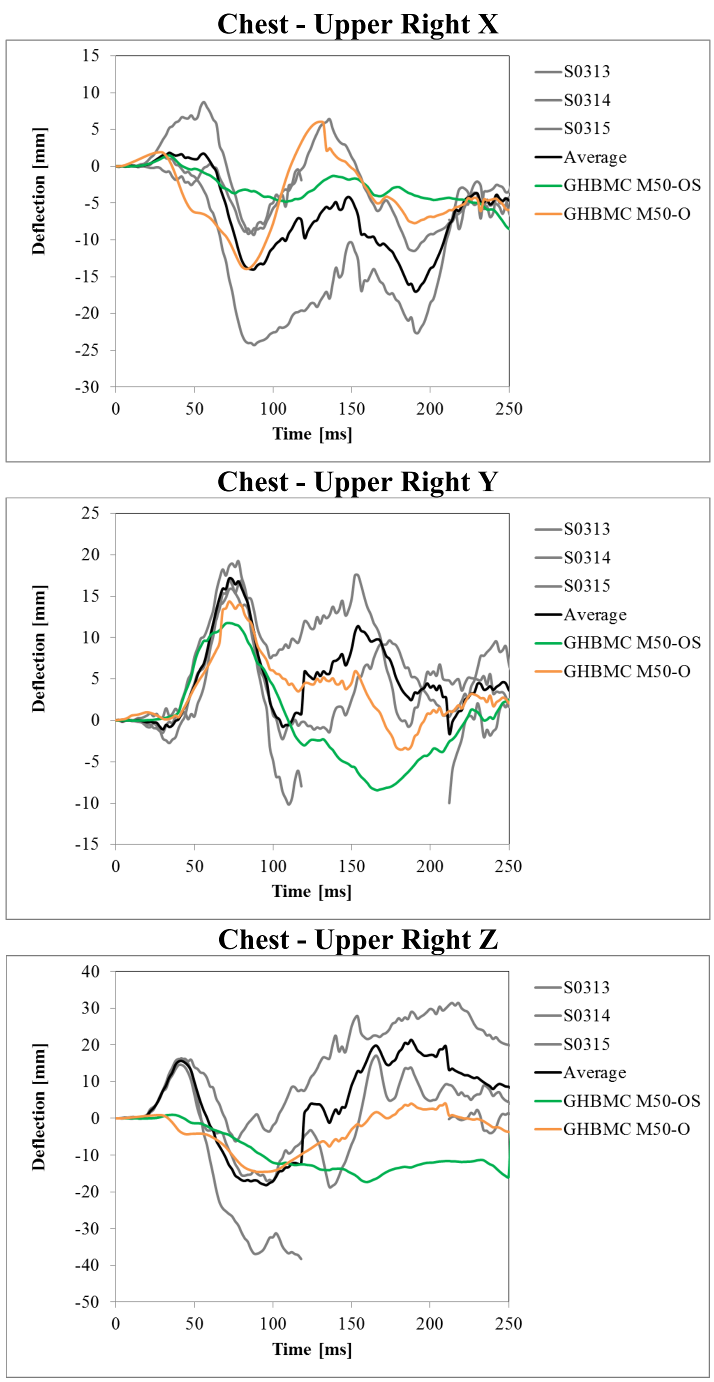

Figure 22. Upper right deflection with respect to the eighth thoracic vertebra (T8), M50-OS, and M50-O, compared to PMHS results.

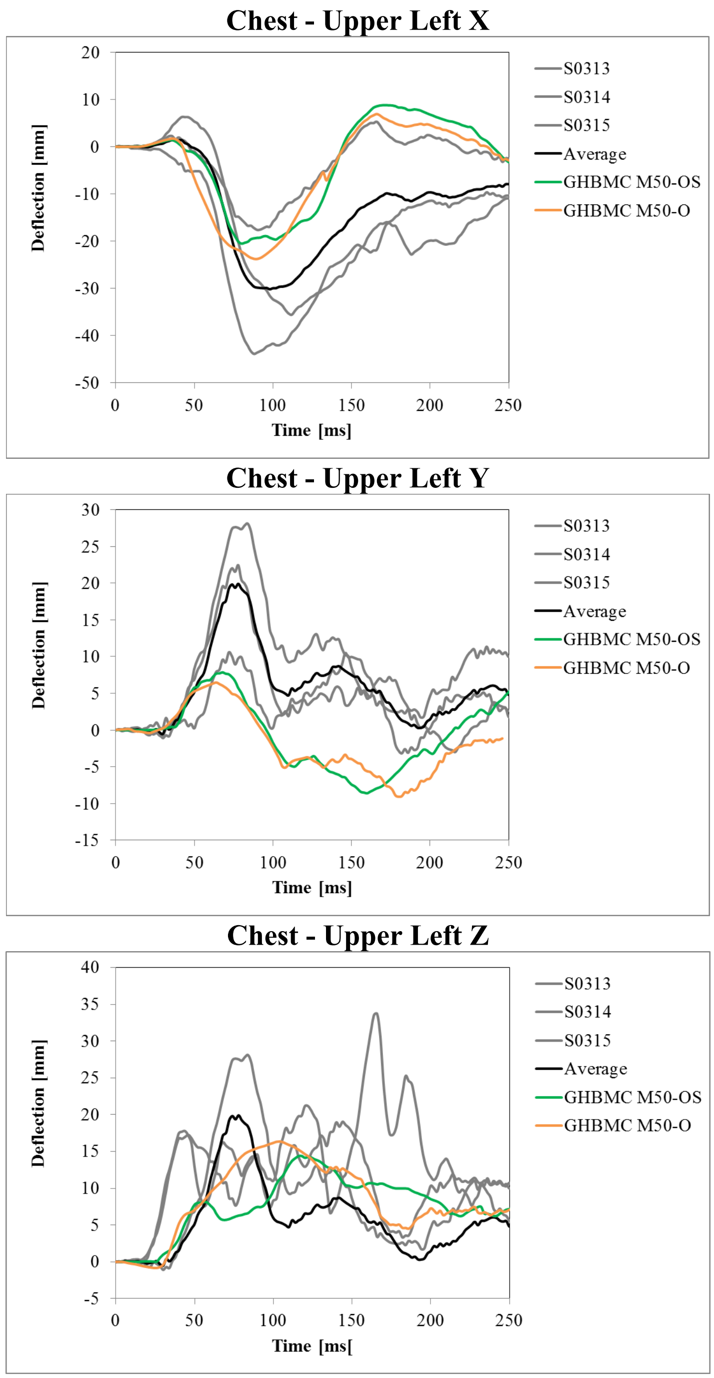

Figure 23. Upper left deflection with respect to the eighth thoracic vertebra (T8), M50-OS, and M50-O, compared to PMHS results.

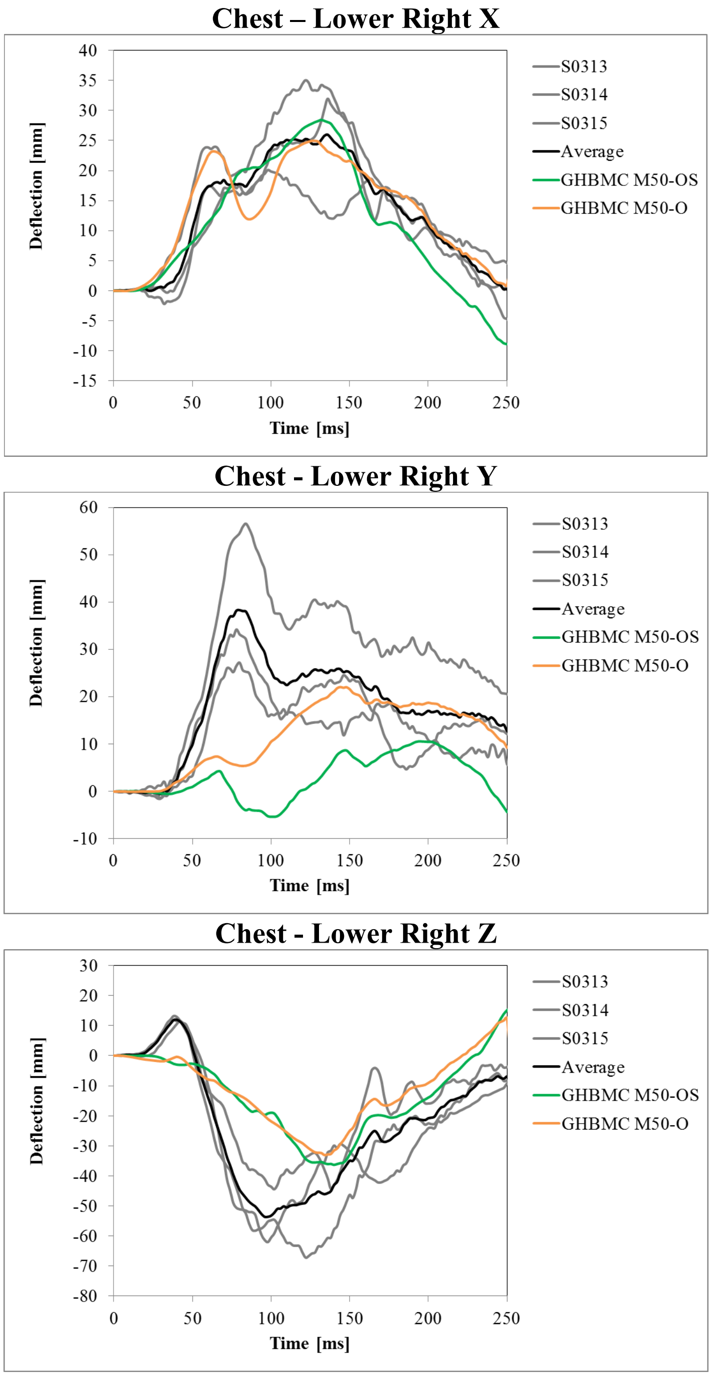

Figure 24. Lower right deflection with respect to the eighth thoracic vertebra (T8), M50-OS, and M50-O, compared to PMHS results.

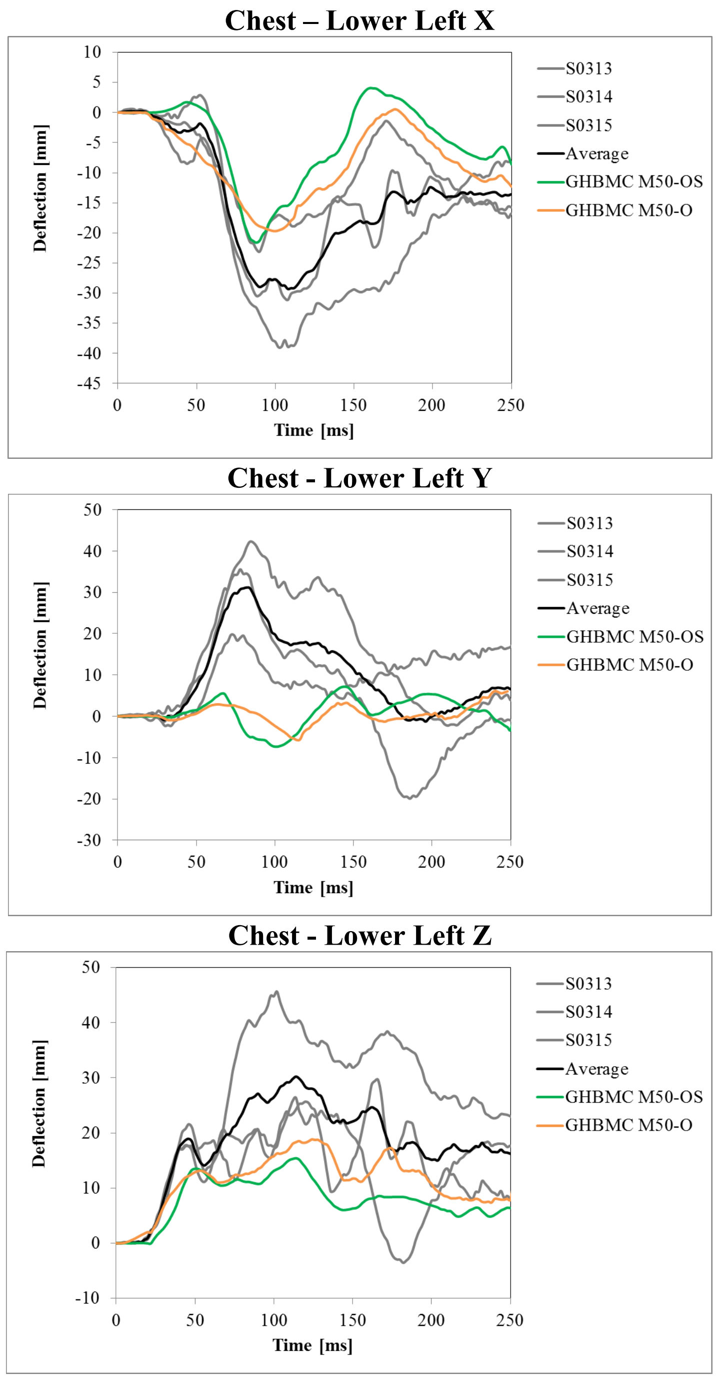

Figure 25. Lower left deflection with respect to the eighth thoracic vertebra (T8), M50-OS, and M50-O, compared to PMHS results.

Table 7. Average peak chest deflection values of PMHS sled test with M50-OS and M50-O simulation data.

	S0313 min/max	S0314 min/max	S0315 min/max	**Average min/max**	*M50-OS min/max*	*M50-O\ min/max*
UL-X	-43.8 0.0	-35.6 6.3	-17.6 5.3	**-32.6** **4.9**	*-20.5* *8.8*	*-23.7* *6.9*
UL-Y	-3.0 22.4	-1.1 28.1	-3.2 10.6	**-4.8** **20.8**	*-8.6* *7.9*	*-9.1* *6.5*
UL-Z	-0.3 33.7	-0.3 32.4	0.0 19.0	**-2.4** **43.7**	*0.0* *14.4*	*-0.8* *16.4*
UR-X	-11.5 6.4	-9.3 8.7	-24.3 1.5	**-13.9** **4.6**	*-8.5* *1.5*	*-13.9* *6.1*
UR-Y	-2.3 19.2	-10.2 15.9	-1.5 17.5	**-7.2** **28.0**	*-8.4* *11.8*	*-3.5* *14.4*
UR-Z	-18.7 17.0	-38.3 16.3	-6.2 31.4	**-37.6** **3.2**	*-13.9* *6.1*	*-14.6* *4.0*
LL-X	-31.1 0.1	-39.0 2.9	-23.1 0.2	**-27.0** **9.8**	*-21.6* *4.1*	*-19.7* *0.6*
LL-Y	-2.2 35.6	-2.3 42.2	-19.9 19.7	**-2.7** **52.9**	*-7.3* *7.2*	*-5.7* *6.2*
LL-Z	0.0 29.7	0.0 45.6	-3.6 26.4	**-4.9** **72.3**	*-19.7* *0.6*	*0.0* *18.8*
LR-X	-2.2 31.9	-4.7 35.0	-0.3 20.1	**-9.7** **32.4**	*-8.9* *28.4*	*0.0* *25.0*
LR-Y	-0.4 34.3	-1.4 56.6	-1.5 27.2	**-7.6** **76.3**	*-5.3* *10.6*	*0.0* *22.1*
LR-Z	-44.4 11.5	-67.2 11.8	-62.0 13.2	**-79.2** **2.9**	*0.0* *25.0*	*-33.1* *12.5*

Injury Assessment

Unlike GHBMC M50-O, the GHBMC M50-OS is not intended to predict crash induced injuries based on tissue-level criterion. The GHBMC M50-OS contains virtual instrumentation such as accelerometers or deflection sensors that we evaluated are meant to be a proxy for test equipment.

GHBMC M50-O simulation results predicted a right clavicle fracture (Figure 26) that was observed in one case (Table 8). No sternum fracture was predicted by the simulations as was the case for two of the three PMHS sled tests (Table 8). However, no cervical fracture was predicted by the model that was observed for only for one of the three subjects (Table 8).

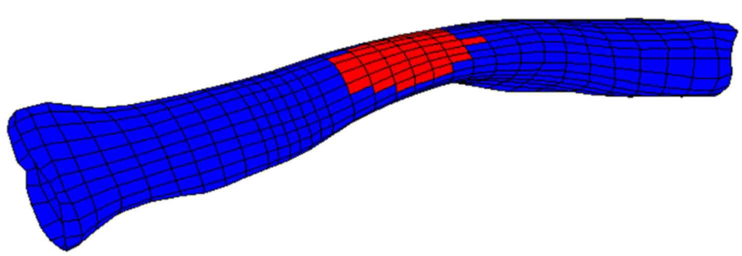

Figure 26. Right clavicle bone fracture predicted by M50-O through post-processing. Red elements are those that exceeded the effective plastic strain failure threshold.

Using the strain-based fracture risk prediction (Forman et al., 2012), the GHBMC 50-O simulations predicted a risk of 85 percent of having at least one rib fracture (Figure 27). This is somewhat consistent with sled tests (two of the three subjects sustained at least one rib fractures). However, two of the three PMHS sled tests obtained seven rib fractures, which is not a risk these simulations predicted (0%).

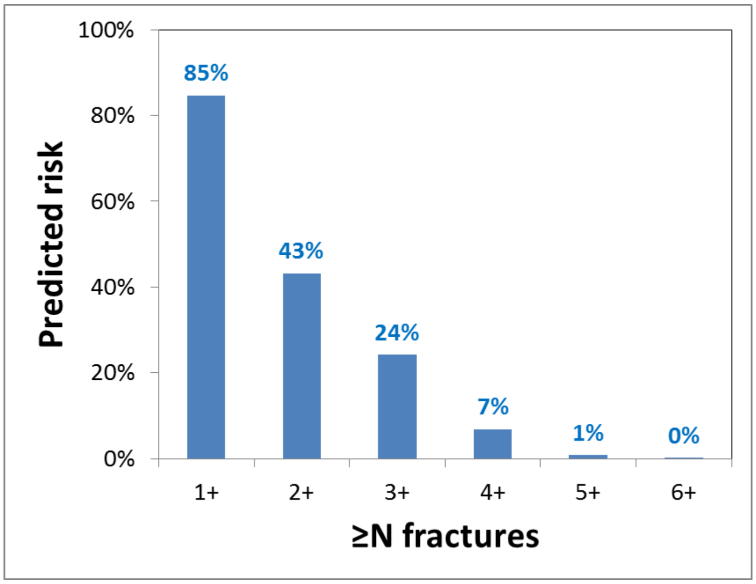

Figure 27. Combined rib fracture probabilities using strain-based fracture risk prediction and an age-adjusted prediction targeting a 60-year-old

Table 8. Summary of injuries predicted by M50-O.

Experiments (n=3)	M50-O	Prediction Method
Clavicle fracture (33%)	Clavicle fx	Post-processing (EPS > 1.78%)
Cervical fracture	None	Post-processing (EPS > 1.78%)
Sternum fracture (33%)	None	Post-processing (EPS > 1.78%)
Rib Fracture (≥ 1) (66 %)	Rib Fracture (≥ 1) (85 %)	Strain-based fracture risk prediction (Forman et al., 2012)
Rib Fracture (≥ 6) (66 %)	Rib Fracture (≥ 6) (0 %)	Strain-based fracture risk prediction (Forman et al., 2012)

Quantitative Evaluation

The CORA rating for each signal is presented in Table 9 and Table 10.

Other Results

Appendix A contains load, moment, and acceleration sensor time histories obtained from the simulations. Also included in Appendix A are subject support and restraint responses. Plots include force and moment time histories for the seat, knee bolster, and footrest load cells.

Table 9. CORA ratings, GHBMC M50-OS.

Signal	Type	Corridor score	Phase score	Magnitude score	Slope score	Correlation score	CORA rating	Model score
Upper Shoulder Belt	Force	0.292	0.800	0.931	0.997	0.909	0.600	
Lower Shoulder Belt	Force	0.139	0.791	0.989	0.993	0.925	0.532	
Lap Belt	Force	0.530	0.742	0.435	0.958	0.712	0.621	0.616
Seat - Resultant	Force	0.376	0.938	0.866	0.977	0.927	0.651	
Kneebolster - Resultant	Force	0.401	1.000	0.497	0.980	0.826	0.614	
Footrest - Resultant	Force	0.411	0.933	0.902	0.996	0.944	0.677	
Upper Thorax [Left] - X	Deflection	0.777	0.659	0.402	0.844	0.635	0.706	
Upper Thorax [Left] - Y	Deflection	0.564	0.388	0.342	0.609	0.446	0.505	0.624
Upper Thorax [Left] - Z	Deflection	0.574	0.930	0.327	0.990	0.749	0.662	
Upper Thorax [Right] - X	Deflection	0.786	0.659	0.143	0.937	0.580	0.683	
Upper Thorax [Right] - Y	Deflection	0.535	0.000	0.930	0.655	0.528	0.532	0.507
Upper Thorax [Right] - Z	Deflection	0.445	0.000	0.001	0.502	0.168	0.306	
Lower Thorax [Left] - X	Deflection	0.441	0.930	0.239	0.909	0.693	0.567	
Lower Thorax [Left] - Y	Deflection	0.729	0.000	0.071	0.806	0.292	0.511	0.570
Lower Thorax [Left] - Z	Deflection	0.537	1.000	0.202	0.983	0.729	0.633	
Lower Thorax [Right] - X	Deflection	0.676	0.840	0.910	0.984	0.911	0.794	
Lower Thorax [Right] - Y	Deflection	0.459	0.000	0.080	0.884	0.321	0.390	0.584
Lower Thorax [Right] - Z	Deflection	0.471	0.659	0.380	0.966	0.669	0.570	
Head - X	Acceleration	0.536	0.168	0.448	0.959	0.525	0.531	
Head - Y	Acceleration	0.643	0.000	0.180	0.666	0.282	0.462	0.520
Head - Z	Acceleration	0.463	0.818	0.207	0.989	0.671	0.567	
T1 - X	Acceleration	0.303	0.969	0.692	0.704	0.788	0.546	
T1 - Y	Acceleration	0.449	0.809	0.104	0.699	0.537	0.493	0.536
T1 - Z	Acceleration	0.347	0.778	0.724	0.873	0.791	0.569	
T8 - X	Acceleration	0.455	0.746	0.641	0.956	0.781	0.618	
T8 - Y	Acceleration	0.460	1.000	0.885	0.864	0.916	0.688	0.663
T8 - Z	Acceleration	0.500	1.000	0.766	0.838	0.868	0.684	
L2 - X	Acceleration	0.495	0.466	0.631	0.949	0.682	0.588	
L2 - Y	Acceleration	0.410	0.675	0.457	0.905	0.679	0.545	0.518
L2 - Z	Acceleration	0.452	0.000	0.500	0.676	0.392	0.422	
Pelvis - X	Acceleration	0.405	1.000	0.970	0.975	0.982	0.693	
Pelvis - Y	Acceleration	0.393	1.000	0.736	0.884	0.873	0.633	0.616
Pelvis - Z	Acceleration	0.515	0.000	0.732	0.852	0.528	0.521	
Head - X	Displacement	0.422	0.884	0.714	0.990	0.863	0.643	
Head - Y	Displacement	0.339	1.000	0.978	0.996	0.991	0.665	0.696
Head - Z	Displacement	0.667	1.000	0.686	0.997	0.894	0.781	
T1 - X	Displacement	0.390	1.000	0.654	1.000	0.885	0.637	
T1 - Y	Displacement	0.733	1.000	0.855	0.998	0.951	0.842	0.619
T1 - Z	Displacement	0.150	0.842	0.222	0.757	0.607	0.379	
T8 - X	Displacement	0.256	0.842	0.527	0.997	0.789	0.522	
T8 - Y	Displacement	0.187	1.000	0.591	0.997	0.863	0.525	0.389
T8 - Z	Displacement	0.048	0.000	0.014	0.554	0.189	0.119	
L2 - X	Displacement	0.400	0.505	0.570	0.957	0.677	0.539	
L2 - Y	Displacement	0.122	1.000	0.256	0.991	0.749	0.435	0.381
L2 - Z	Displacement	0.165	0.000	0.003	0.512	0.171	0.168	
Pelvis - X	Displacement	0.692	0.842	0.643	0.937	0.807	0.750	
Pelvis - Y	Displacement	0.130	0.674	0.152	0.922	0.583	0.356	0.487
Pelvis - Z	Displacement	0.266	0.337	0.044	0.949	0.443	0.354	
Shoulder [Left] - X	Displacement	0.188	1.000	0.555	0.998	0.851	0.520	
Shoulder [Left] - Y	Displacement	0.243	1.000	0.531	0.998	0.843	0.543	0.467
Shoulder [Left] - Z	Displacement	0.043	1.000	0.068	0.829	0.633	0.338	
Shoulder [Right] - X	Displacement	0.219	1.000	0.415	0.999	0.804	0.512	
Shoulder [Right] - Y	Displacement	0.294	1.000	0.603	0.999	0.867	0.580	0.497
Shoulder [Right] - Z	Displacement	0.146	1.000	0.025	0.925	0.650	0.398	

Table 10. CORA ratings, GHBMC M50-O.

Signal	Type	Corridor score	Phase score	Magnitude score	Slope score	Correlation score	CORA rating	Model score
Upper Shoulder Belt	Force	0.413	0.895	0.918	0.998	0.936	0.675	0.641
Lower Shoulder Belt	Force	0.240	0.930	0.978	0.995	0.968	0.604	
Lap Belt	Force	0.417	0.914	0.488	0.972	0.791	0.604	
Seat - Resultant	Force	0.237	0.923	0.927	0.981	0.944	0.590	
Kneebolster - Resultant	Force	0.635	0.893	0.562	0.984	0.813	0.724	
Footrest - Resultant	Force	0.444	0.942	0.621	0.988	0.850	0.647	
Upper Thorax [Left] - X	Deflection	0.574	0.886	0.766	0.942	0.865	0.719	0.732
Upper Thorax [Left] - Y	Deflection	0.726	0.796	0.762	0.864	0.807	0.767	
Upper Thorax [Left] - Z	Deflection	0.559	0.882	0.710	0.995	0.862	0.711	
Upper Thorax [Right] - X	Deflection	0.556	0.557	0.664	0.860	0.694	0.625	0.612
Upper Thorax [Right] - Y	Deflection	0.525	0.400	0.754	0.869	0.674	0.600	
Upper Thorax [Right] - Z	Deflection	0.527	0.649	0.633	0.810	0.697	0.612	
Lower Thorax [Left] - X	Deflection	0.287	0.701	0.593	0.965	0.753	0.520	0.599
Lower Thorax [Left] - Y	Deflection	0.541	0.667	0.491	0.918	0.692	0.617	
Lower Thorax [Left] - Z	Deflection	0.462	1.000	0.576	0.991	0.856	0.659	
Lower Thorax [Right] - X	Deflection	0.543	0.280	0.751	0.970	0.667	0.605	0.615
Lower Thorax [Right] - Y	Deflection	0.614	0.000	0.423	0.950	0.458	0.536	
Lower Thorax [Right] - Z	Deflection	0.670	0.625	0.617	0.974	0.739	0.704	
Head - X	Acceleration	0.207	0.056	0.162	0.679	0.299	0.253	0.351
Head - Y	Acceleration	0.301	0.079	0.431	0.669	0.393	0.347	
Head - Z	Acceleration	0.217	0.634	0.574	0.864	0.691	0.454	
T1 - X	Acceleration	0.482	0.323	0.261	0.735	0.440	0.461	0.597
T1 - Y	Acceleration	0.807	0.607	0.495	0.871	0.658	0.732	
T1 - Z	Acceleration	0.598	0.259	0.775	0.761	0.598	0.598	
T8 - X	Acceleration	0.604	0.812	0.600	0.947	0.786	0.703	0.716
T8 - Y	Acceleration	0.651	0.831	0.712	0.871	0.805	0.728	
T8 - Z	Acceleration	0.525	0.962	0.743	0.895	0.867	0.718	
L2 - X	Acceleration	0.710	0.686	0.607	0.949	0.747	0.728	0.642
L2 - Y	Acceleration	0.566	0.225	0.505	0.919	0.550	0.558	
L2 - Z	Acceleration	0.804	0.453	0.241	0.741	0.478	0.641	
Pelvis - X	Acceleration	0.137	0.839	0.654	0.986	0.826	0.482	0.532
Pelvis - Y	Acceleration	0.176	1.000	0.750	0.960	0.903	0.540	
Pelvis - Z	Acceleration	0.347	0.618	0.853	0.945	0.805	0.576	
Head - X	Displacement	0.532	0.968	0.738	0.993	0.900	0.716	0.759
Head - Y	Displacement	0.578	1.000	0.963	0.999	0.987	0.783	
Head - Z	Displacement	0.687	1.000	0.614	0.999	0.871	0.779	
T1 - X	Displacement	0.709	1.000	0.856	1.000	0.952	0.831	0.801
T1 - Y	Displacement	0.821	1.000	0.953	0.999	0.984	0.903	
T1 - Z	Displacement	0.515	1.000	0.611	0.861	0.824	0.669	
T8 - X	Displacement	0.232	1.000	0.430	0.999	0.810	0.521	0.432
T8 - Y	Displacement	0.069	1.000	0.593	0.998	0.864	0.466	
T8 - Z	Displacement	0.034	0.758	0.021	0.982	0.587	0.310	
L2 - X	Displacement	0.957	0.842	0.855	0.995	0.897	0.927	0.685
L2 - Y	Displacement	0.287	1.000	0.384	0.993	0.792	0.540	
L2 - Z	Displacement	0.475	0.842	0.276	0.996	0.705	0.590	
Pelvis - X	Displacement	0.811	0.968	0.853	0.969	0.930	0.870	0.520
Pelvis - Y	Displacement	0.113	0.842	0.267	0.952	0.687	0.400	
Pelvis - Z	Displacement	0.269	0.000	0.094	0.827	0.307	0.288	
Shoulder [Left] - X	Displacement	0.228	0.632	0.448	0.988	0.689	0.458	0.562
Shoulder [Left] - Y	Displacement	0.204	1.000	0.565	0.995	0.853	0.529	
Shoulder [Left] - Z	Displacement	0.495	1.000	0.813	0.901	0.905	0.700	
Shoulder [Right] - X	Displacement	0.021	0.716	0.098	0.996	0.603	0.312	0.377
Shoulder [Right] - Y	Displacement	0.073	0.842	0.477	0.989	0.769	0.421	
Shoulder [Right] - Z	Displacement	0.146	1.000	0.025	0.925	0.650	0.398	

2.2 THOR FE

Model Stability Assessment

Instability was observed in the shoulder pad during the belt interaction (Figure 28). This led to a negative volume error. This issue occurred even with the *CONTACT_INTERIOR definition. It is possible that contact interior failed to stabilize the element deformation because the deforming node fell outside of the contact interior surface definition (opposite element wall for tetras). Increasing the stiffness of the shoulder pads solved this issue.

No other instability was reported after the shoulder pad stiffness was increased.

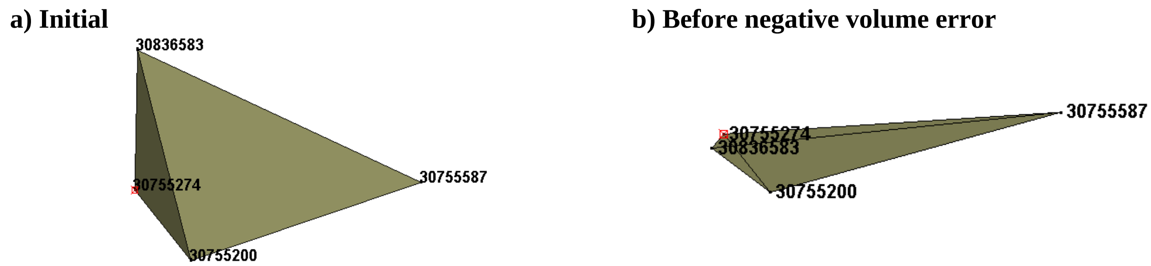

Figure 28. Instability in the shoulder pad, THOR FE.

Shoulder Belt Loads

Upper shoulder belt force - time histories are provided in Figure 29.

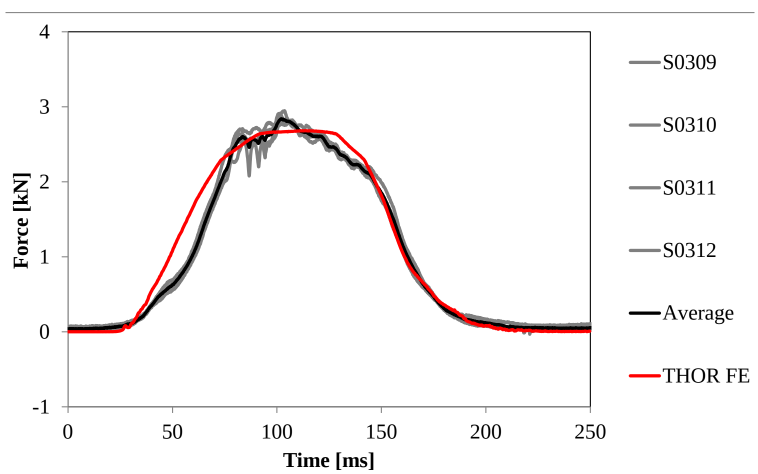

Figure 29. Upper shoulder belt loads obtained by THOR FE.

Occupant Kinematics

Motions of the head, spine, shoulders, and pelvis are provided in Figure 30 to Figure 38 relative to the buck. Peak excursion values for all measurements locations in the X, Y, and Z-axis directions are provided in Table 11.

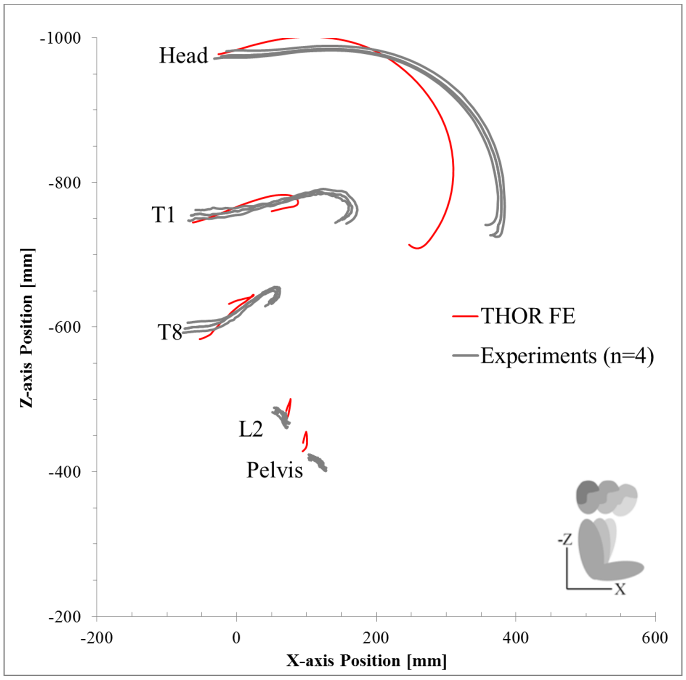

Figure 30. Spine trajectory for THOR FE relative to THOR dummy sled test response (lateral view)

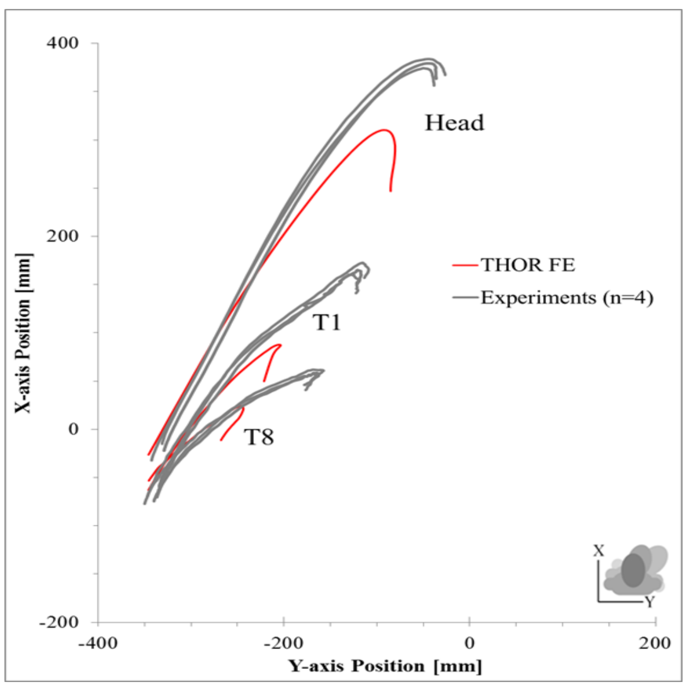

Figure 31. Spine trajectory for THOR FE relative to THOR sled test response (top view)

Table 11. Peak excursions 0-175ms, THOR FE.

		X		Y		Z	
		Min	**Max**	**Min**	**Max**	**Min**	**Max**
Head	S0309	0	407	0	306	-12	230
	S0310	0	401	0	295	-10	247
	S0311	0	416	0	297	-14	243
	S0312	0	399	0	306	-7	257
	average	**0**	**406**	**0**	**301**	**-11**	**244**
	st dev	**0**	**8**	**0**	**6**	**3**	**11**
	THOR FE	*0*	*337*	*0*	*265*	*-24*	*268*
L Shoulder	S0309	0	302	0	255	-93	1
	S0310	0	310	0	243	-79	0
	S0311	0	328	0	249	-89	0
	S0312	0	318	-1	255	-70	0
	average	**0**	**314**	**0**	**251**	**-83**	**0**
	st dev	**0**	**11**	**0**	**6**	**10**	**1**
	THOR FE	*0*	*249*	*0*	*176*	*-92*	*0*
R Shoulder	S0309	0	332	-1	211	-22	48
	S0310	0	329	-1	212	-14	59
	S0311	-1	339	-1	201	-21	60
	S0312	-3	323	-5	222	-17	62
	average	**-1**	**331**	**-2**	**212**	**-18**	**57**
	st dev	**1**	**7**	**2**	**8**	**3**	**6**
	THOR FE	*-1*	*264*	*0*	*167*	*-13*	*59*
T1	S0309	0	230	0	227	-38	6
	S0310	0	231	0	219	-33	9
	S0311	0	236	0	222	-39	7
	S0312	0	232	0	226	-19	20
	average	**0**	**232**	**0**	**223**	**-35**	**11**
	st dev	**0**	**3**	**0**	**4**	**5**	**6**
	THOR FE	*-3*	*151*	*0*	*142*	*-38*	*0*
T8	S0309	0	135	0	184	-58	0
	S0310	0	133	0	178	-57	0
	S0311	0	133	0	179	-60	0
	S0312	0	132	0	179	-50	0
	average	**0**	**133**	**0**	**180**	**-56**	**0**
	st dev	**0**	**1**	**0**	**3**	**5**	**0**
	THOR FE	*-17*	*77*	*0*	*102*	*-61*	*0*
L2	S0309	0	22	0	79	-2	22
	S0310	0	17	0	80	0	22
	S0311	0	19	0	82	-2	15
	S0312	0	20	0	84	0	22
	average	**0**	**19**	**0**	**81**	**-1**	**20**
	st dev	**0**	**2**	**0**	**2**	**1**	**4**
	THOR FE	*-1*	*37*	*0*	*59*	*-33*	*0*
Pelvis	S0309	0	32	0	66	-2	19
	S0310	0	28	0	69	0	20
	S0311	-4	26	0	71	-2	14
	S0312	0	32	0	74	0	20
	average	**-1**	**29**	**0**	**70**	**-1**	**18**
	st dev	**2**	**3**	**0**	**4**	**1**	**3**
	THOR FE	*-3*	*21*	*0*	*44*	*-27*	*0*

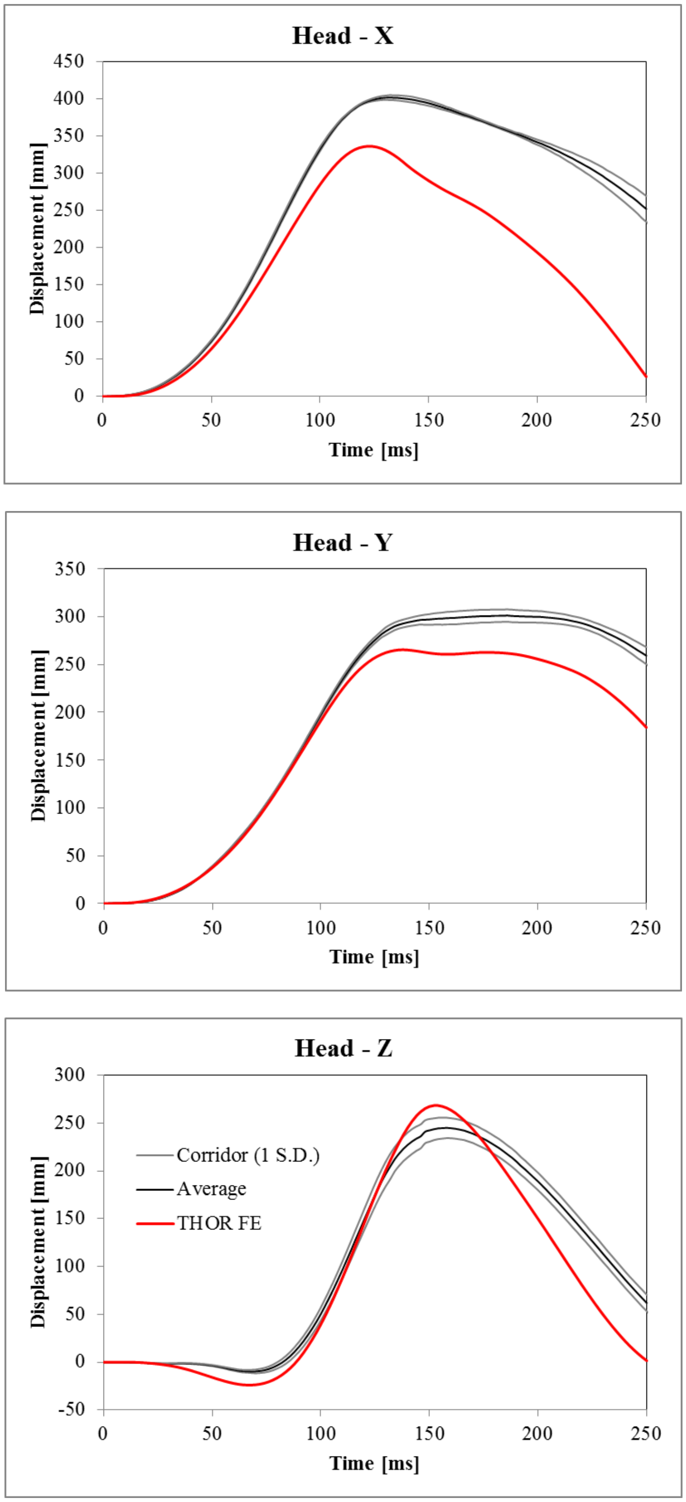

Figure 32. Displacements of the THOR head relative to the buck

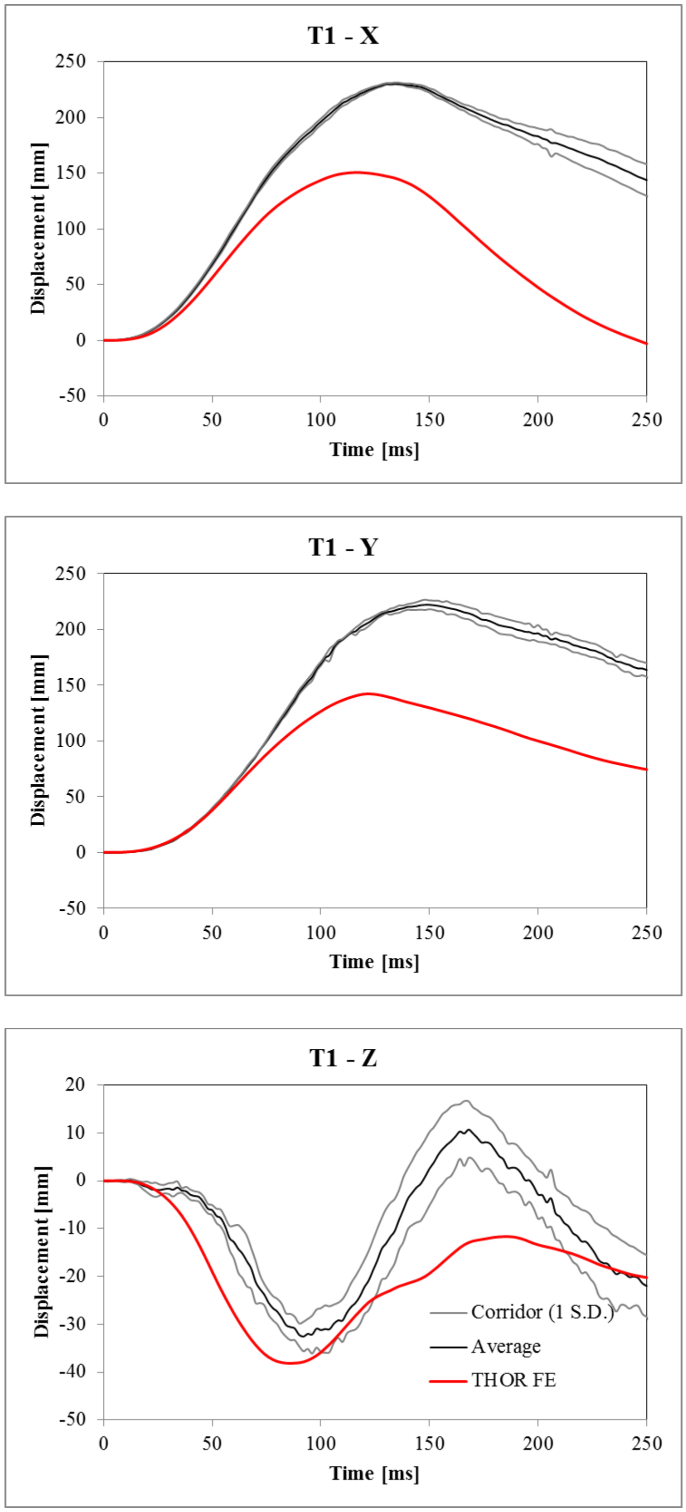

Figure 33. Displacements of the THOR T1 relative to the buck

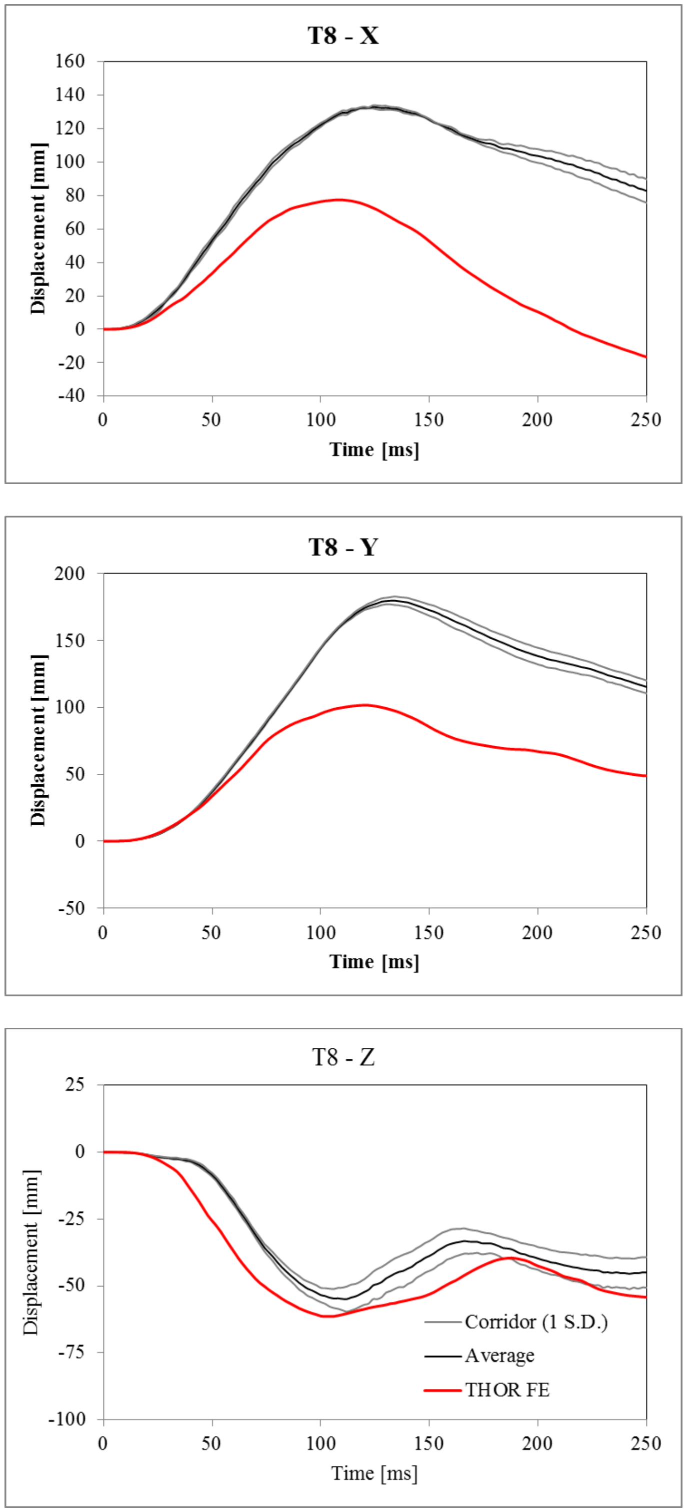

Figure 34. Displacements of the THOR T8 relative to the buck

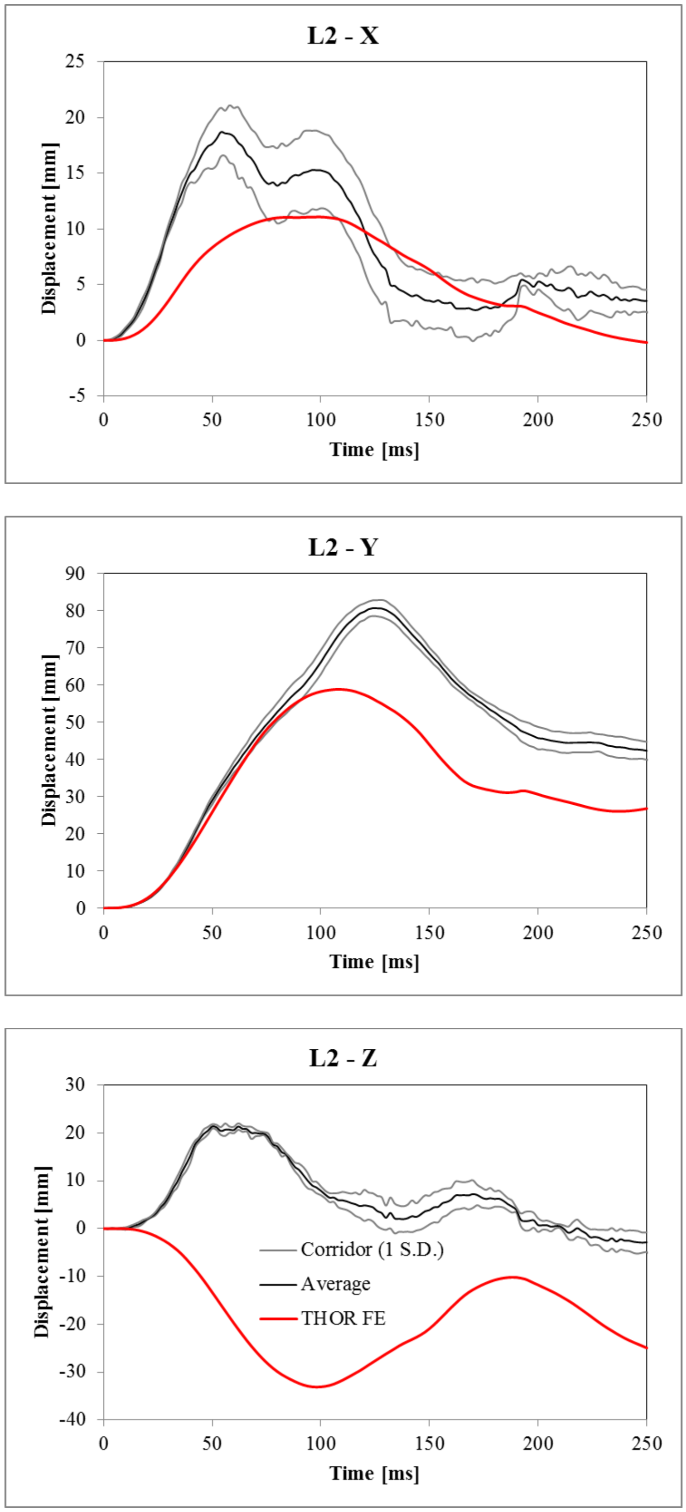

Figure 35. Displacements of the THOR L2 relative to the buck

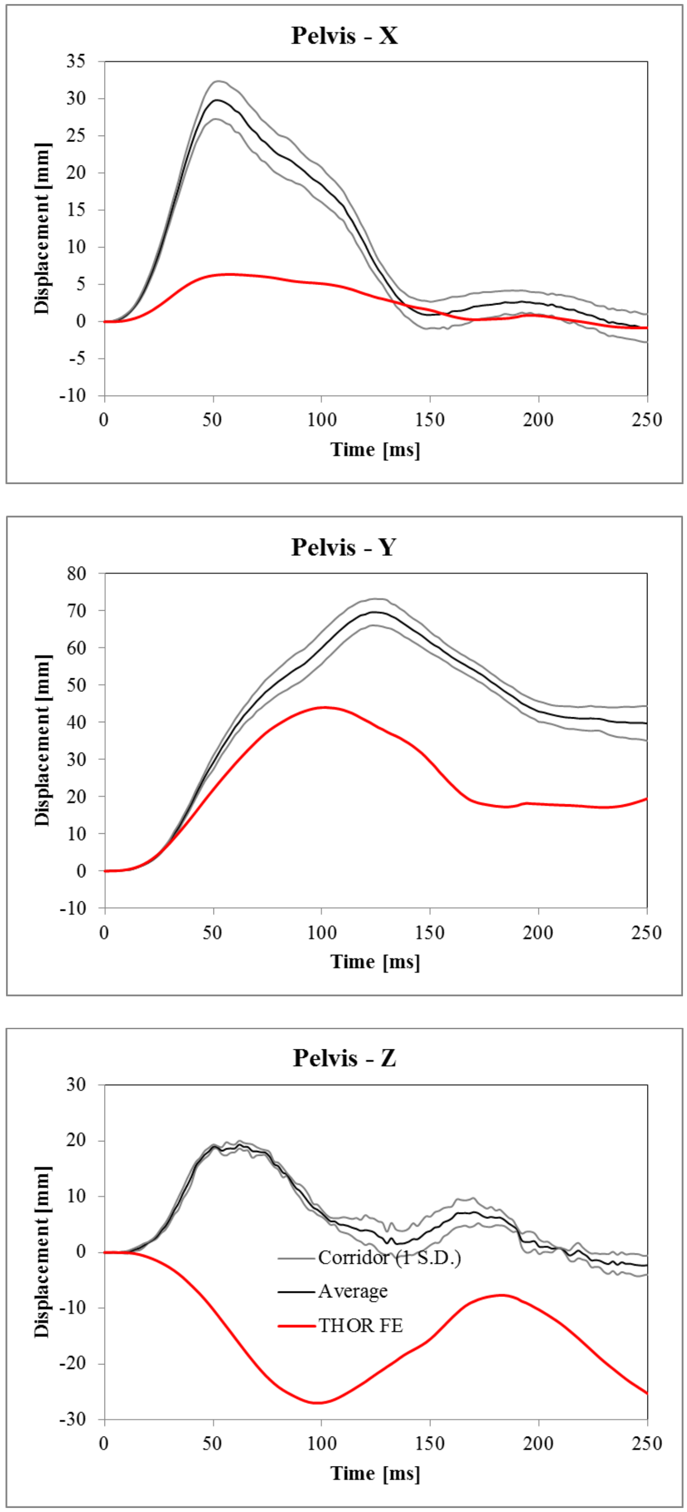

Figure 36. Displacements of the THOR pelvis relative to the buck

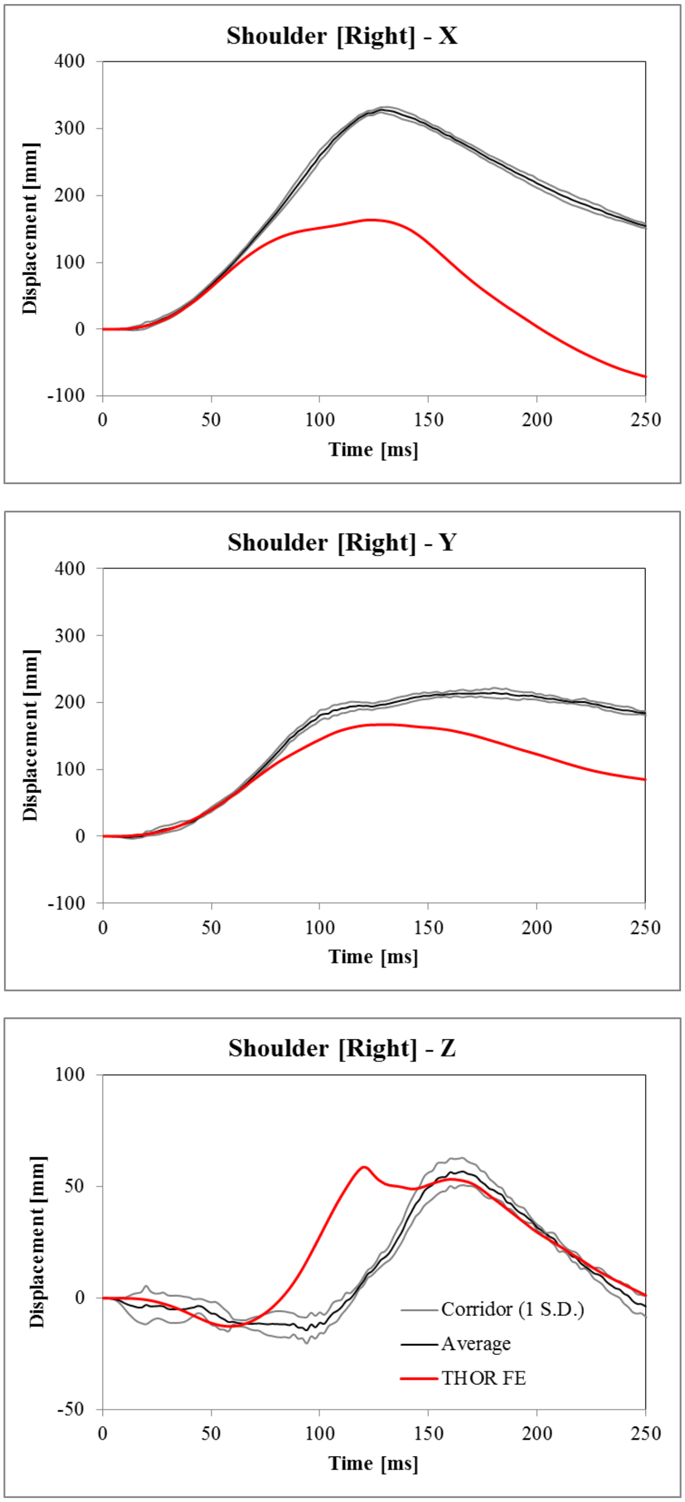

Figure 37. Displacements of the THOR right shoulder relative to the buck

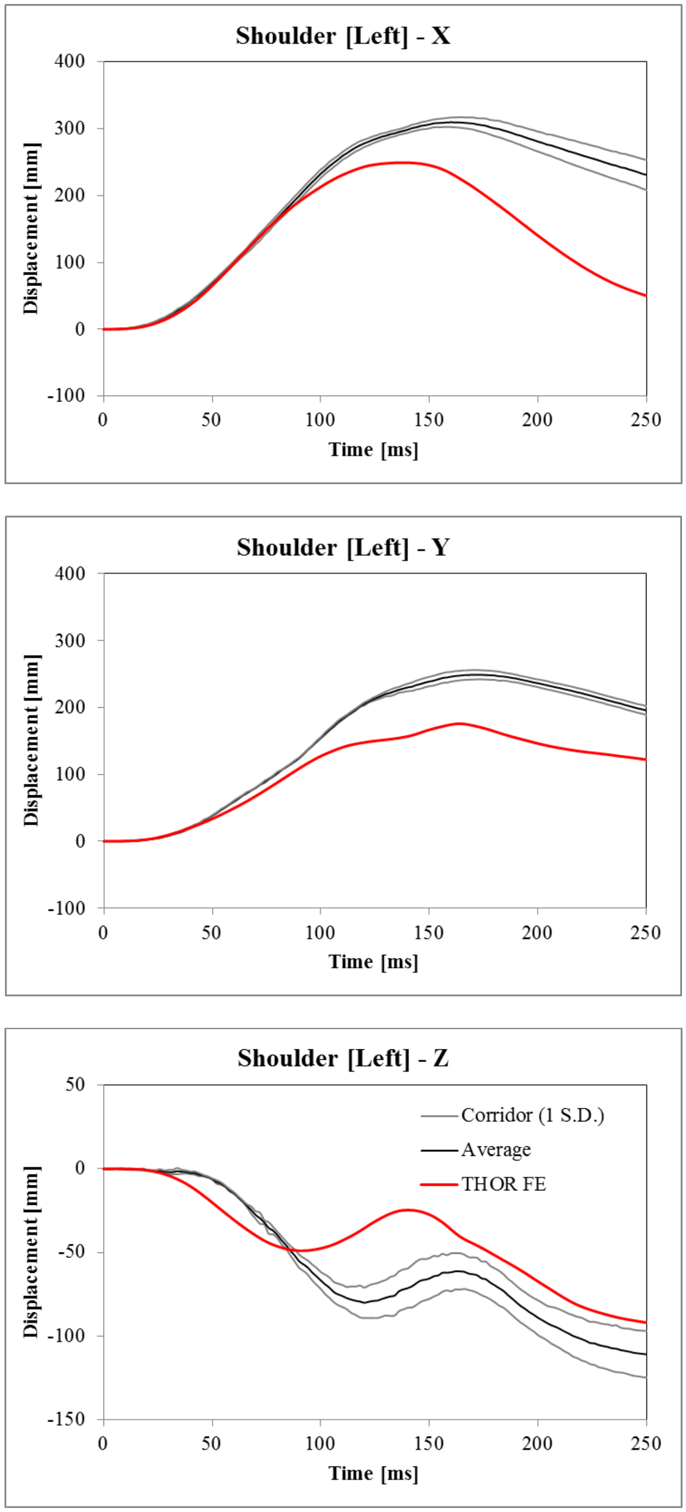

Figure 38. Displacements of the THOR left shoulder relative to the buck

Accelerations

Selected accelerations time histories are shown in Figure 39. While excellent fit was observed for the pelvis acceleration, significant differences in head accelerations were observed. Spikes in the head sensor traces in the FE model were caused by a direct impact of the head to the clavicle (Figure 40), which did not occur in the experiments.

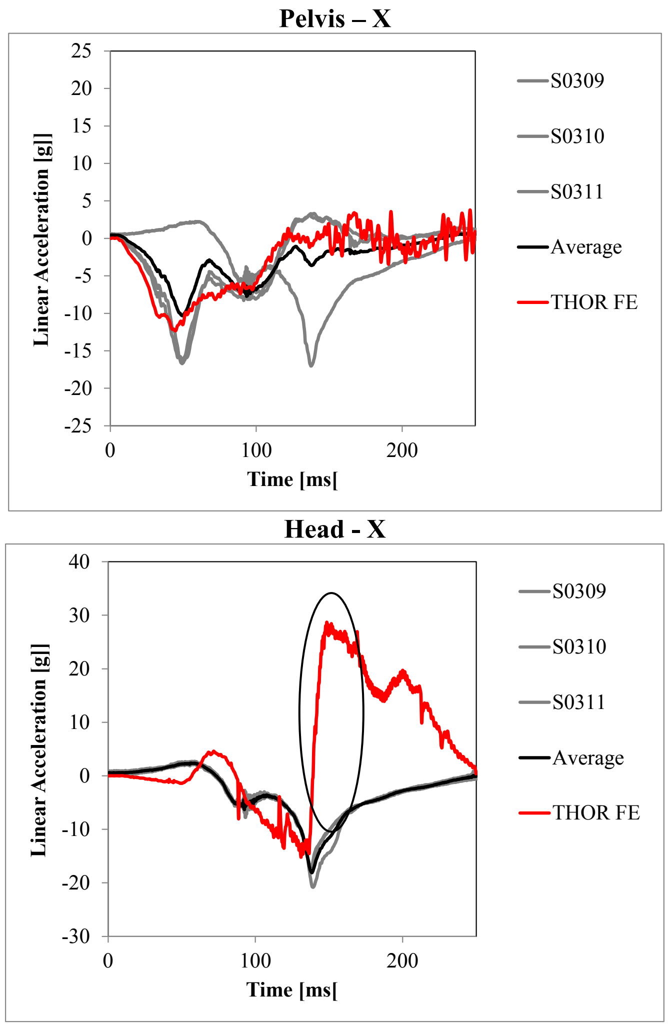

Figure 39. THOR sensor time-history plots for head and pelvis

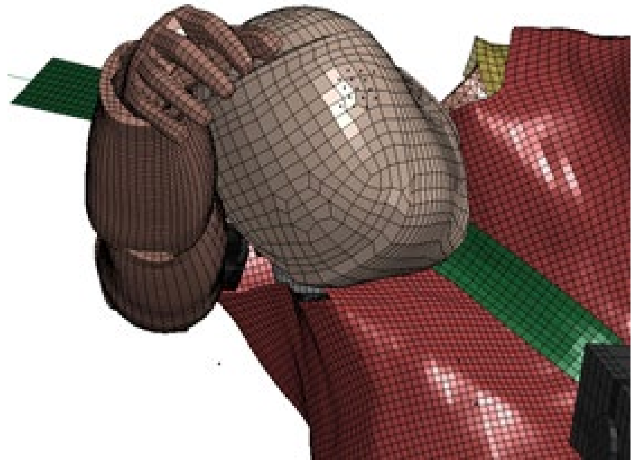

Figure 40. THOR FE head impacting clavicle at 129 ms

Chest Deflection

Processed IR-TRACC deflection time-history plots are provided in Figure 41. Average peak IR-TRACC X, Y, and Z-axis deflection values are presented in Table 12.

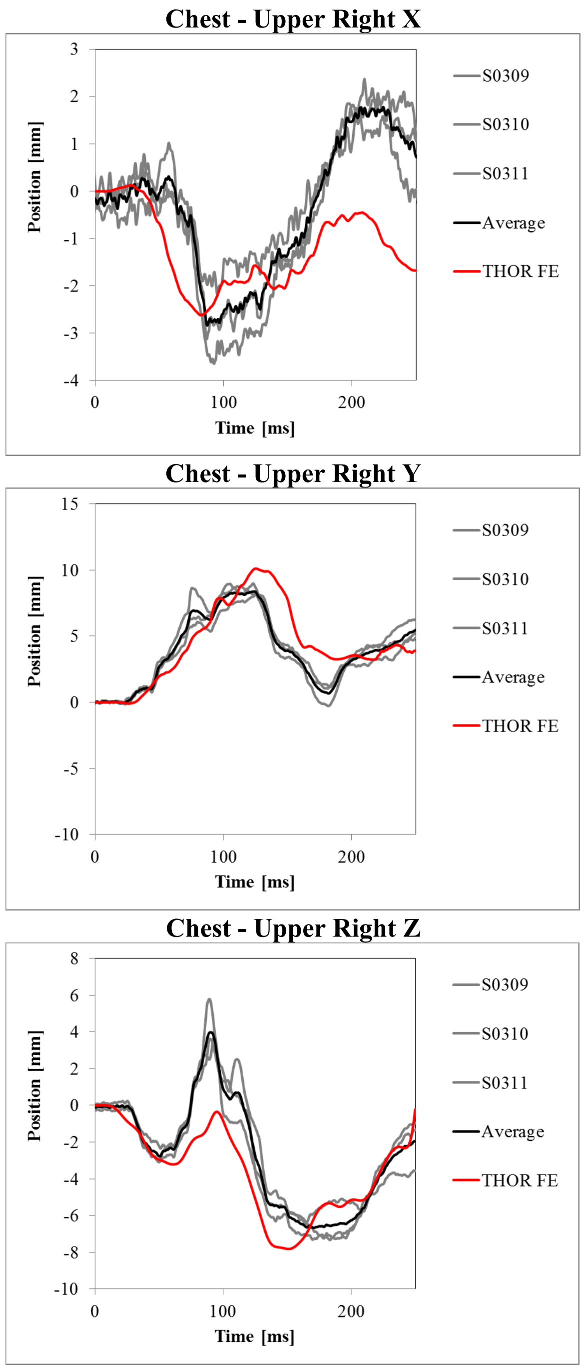

Figure 41. THOR IR-TRACC upper right deflection time histories

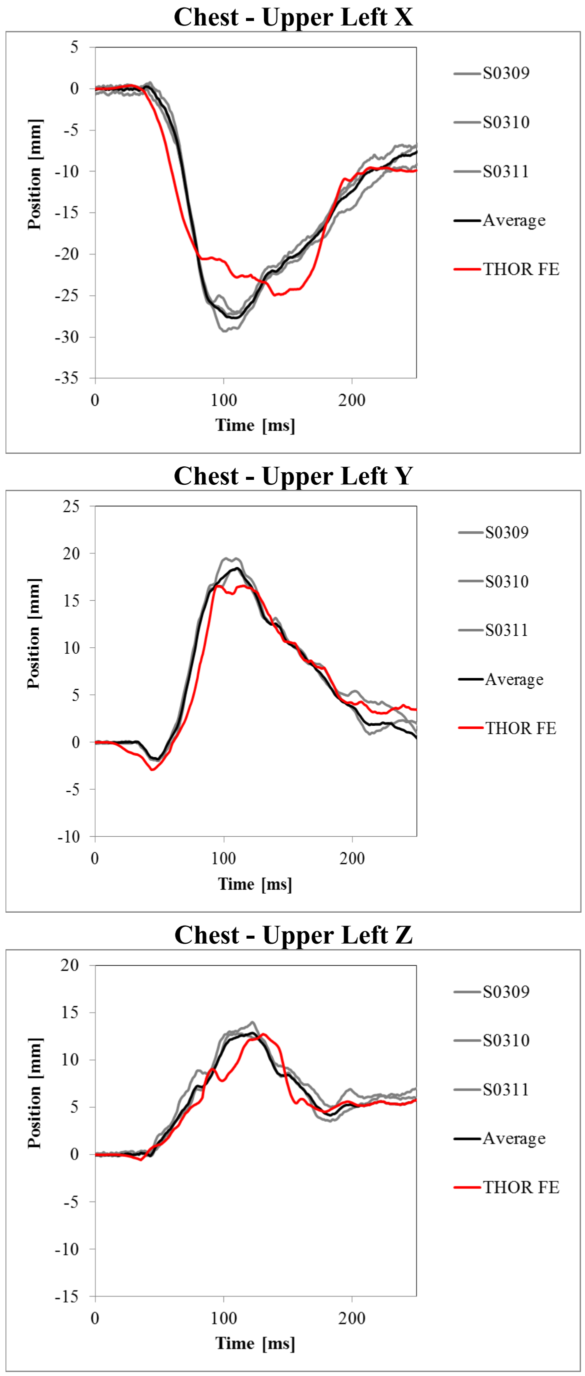

Figure 42. THOR IR-TRACC upper left deflection time histories

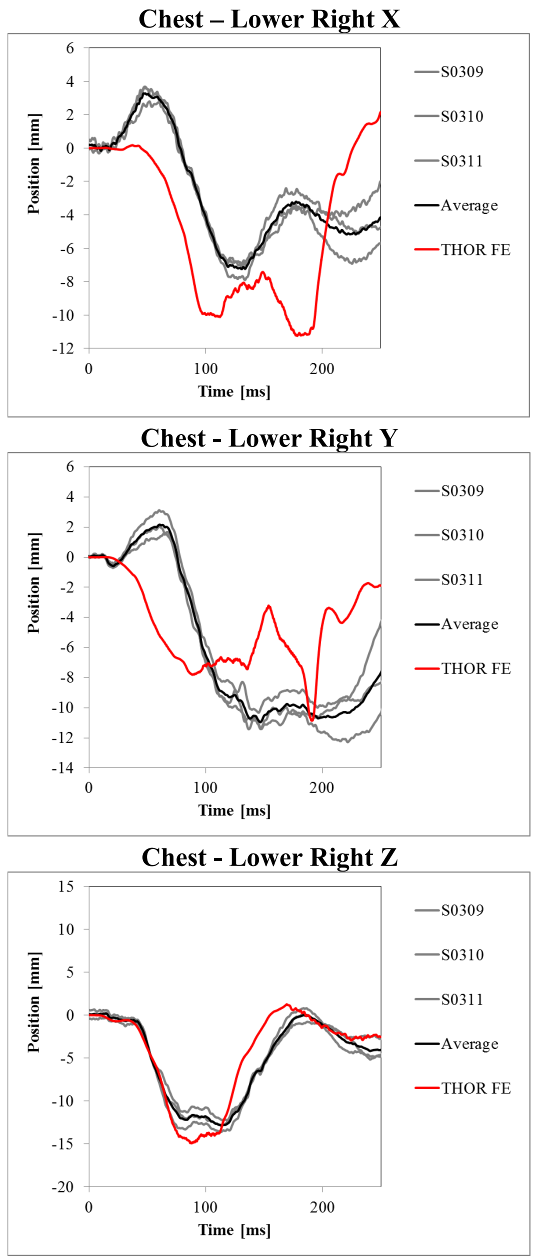

Figure 43. THOR IR-TRACC lower right deflection time histories

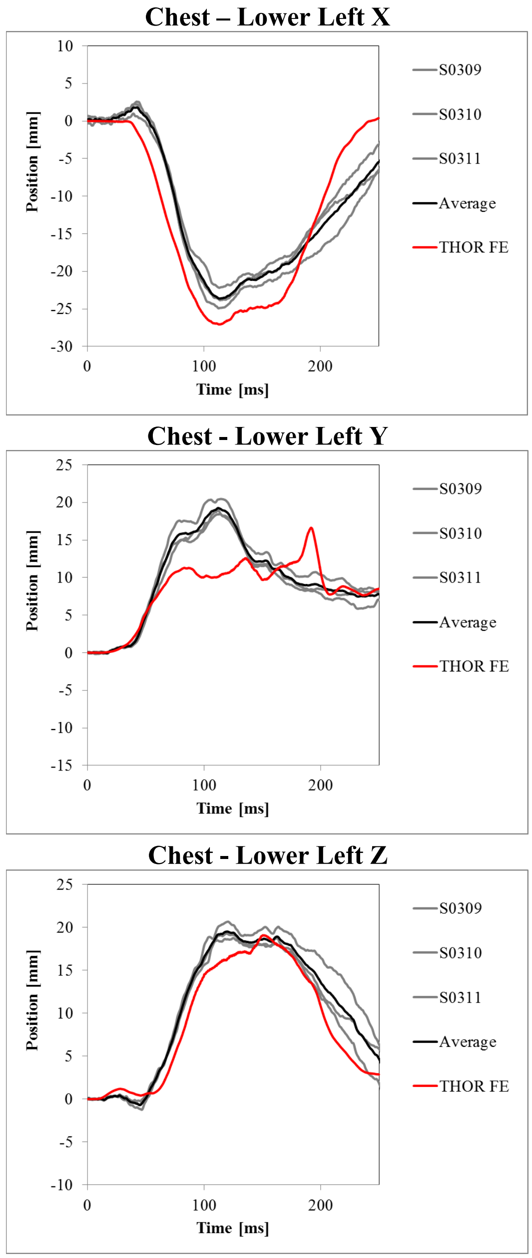

Figure 44. THOR IR-TRACC lower left deflection time histories

Table 12. Average Peak IR-TRACC X, Y, and Z-axis deflection values, THOR FE.

	S0309 min/max	S0310 min/max	S0311 min/max	S0312 min/max	**Average min/max**	*THOR FE min/max*
UL-X	-26.9 0.3	-27.0 0.8	-29.6 0.3	-28.8 0.6	**-28.1** **0.5**	*-25.0* *0.4*
UL-Y	-0.3 12.4	0.1 13.0	-0.1 13.9	-0.2 11.7	**-0.1** **12.7**	*-2.9* *12.7*
UL-Z	-1.5 17.5	-1.9 18.5	-2.0 19.5	-2.1 19.4	**-1.9** **18.7**	*-6.2* *16.6*
UR-X	-3.2 1.8	-2.0 1.9	-3.3 1.7	-3.5 1.4	**-3.0** **1.7**	*-2.6* *0.1*
UR-Y	-0.1 8.2	-0.3 9.0	0.0 9.1	-0.8 7.0	**-0.3** **8.3**	*-0.1* *10.1*
UR-Z	7.5 3.6	6.1 6.0	7.2 3.7	8.2 4.1	**-7.2** **4.4**	*-7.8* *0.0*
LL-X	-23.6 1.2	-22.4 2.4	-25.4 1.7	-24.3 2.3	**-23.9** **1.9**	*-27.1* *0.4*
LL-Y	-0.2 18.3	0.0 18.9	-0.1 20.5	-0.1 18.4	**-0.1** **19.1**	*0.0* *16.6*
LL-Z	0.2 19.3	-1.2 18.8	-0.8 20.6	-1.9 20.4	**-0.9** **19.8**	*0.0* *19.1*
LR-X	-7.1 3.0	-6.9 3.6	-7.9 3.7	-8.6 3.3	**-7.6** **3.4**	*-11.2* *2.2*
LR-Y	-7.2 2.1	-6.9 0.1	-8.3 3.3	-8.5 3.4	**-7.7** **3.3**	*-10.9* *0.0*
LR-Z	-11.4 1.6	-10.4 3.0	-11.7 2.0	-12.0 1.6	**-11.4** **2.1**	*-14.9* *1.3*

Quantitative Evaluation

The CORA rating for each signal is presented in Table 13. Except for head acceleration, displacements of head, T1, T8, L2, and both shoulders, all other outputs display fair correlation.

Table 13. CORA ratings, THOR FE.

Signal	Type	Corridor score	Phase score	Magnitude score	Slope score	Correlation score	CORA rating	Model score
Upper Shoulder Belt	Force	0.474	0.942	0.911	0.998	0.950	0.712	
Lower Shoulder Belt	Force	0.290	1.000	0.972	0.995	0.989	0.640	
Lap Belt	Force	0.360	1.000	0.514	0.979	0.831	0.596	0.653
Seat - Resultant	Force	0.168	0.915	0.958	0.983	0.952	0.560	
Kneebolster - Resultant	Force	0.752	0.840	0.594	0.986	0.807	0.779	
Footrest - Resultant	Force	0.461	0.947	0.481	0.984	0.804	0.632	
Upper Thorax [Left] - X	Deflection	0.472	1.000	0.948	0.991	0.980	0.726	
Upper Thorax [Left] - Y	Deflection	0.807	1.000	0.971	0.992	0.988	0.897	0.786
Upper Thorax [Left] - Z	Deflection	0.551	0.858	0.902	0.997	0.919	0.735	
Upper Thorax [Right] - X	Deflection	0.441	0.506	0.925	0.821	0.751	0.596	
Upper Thorax [Right] - Y	Deflection	0.521	0.600	0.666	0.977	0.747	0.634	0.665
Upper Thorax [Right] - Z	Deflection	0.568	0.973	0.949	0.964	0.962	0.765	
Lower Thorax [Left] - X	Deflection	0.211	0.586	0.770	0.994	0.783	0.497	
Lower Thorax [Left] - Y	Deflection	0.448	1.000	0.701	0.975	0.892	0.670	0.613
Lower Thorax [Left] - Z	Deflection	0.425	1.000	0.763	0.994	0.919	0.672	
Lower Thorax [Right] - X	Deflection	0.476	0.000	0.672	0.962	0.545	0.511	
Lower Thorax [Right] - Y	Deflection	0.691	0.000	0.595	0.982	0.526	0.608	0.630
Lower Thorax [Right] - Z	Deflection	0.770	0.608	0.736	0.978	0.774	0.772	
Head - X	Acceleration	0.043	0.000	0.020	0.538	0.186	0.114	
Head - Y	Acceleration	0.129	0.119	0.557	0.670	0.449	0.289	0.267
Head - Z	Acceleration	0.094	0.542	0.757	0.802	0.700	0.397	
T1 - X	Acceleration	0.572	0.000	0.046	0.751	0.266	0.419	
T1 - Y	Acceleration	0.985	0.506	0.690	0.958	0.718	0.852	0.628
T1 - Z	Acceleration	0.724	0.000	0.800	0.705	0.502	0.613	
T8 - X	Acceleration	0.678	0.845	0.580	0.942	0.789	0.745	
T8 - Y	Acceleration	0.747	0.747	0.625	0.874	0.749	0.748	0.743
T8 - Z	Acceleration	0.538	0.943	0.732	0.924	0.866	0.735	
Pelvis - X	Acceleration	0.817	0.795	0.595	0.949	0.780	0.799	
Pelvis - Y	Acceleration	0.644	0.000	0.529	0.926	0.485	0.564	0.704
Pelvis - Z	Acceleration	0.980	0.680	0.111	0.773	0.521	0.750	
Head - X	Displacement	0.003	0.758	0.496	0.992	0.749	0.376	
Head - Y	Displacement	0.068	1.000	0.757	0.999	0.919	0.493	0.491
Head - Z	Displacement	0.263	0.926	0.913	0.992	0.944	0.603	
T1 - X	Displacement	0.001	0.505	0.307	0.980	0.597	0.299	
T1 - Y	Displacement	0.142	0.968	0.361	0.992	0.774	0.458	0.459
T1 - Z	Displacement	0.419	1.000	0.530	0.924	0.818	0.619	
T8 - X	Displacement	0.015	0.337	0.207	0.960	0.501	0.258	
T8 - Y	Displacement	0.059	0.884	0.295	0.992	0.724	0.391	0.422
T8 - Z	Displacement	0.342	1.000	0.676	0.995	0.890	0.616	
L2 - X	Displacement	0.487	0.758	0.486	0.982	0.742	0.614	
L2 - Y	Displacement	0.208	0.968	0.535	0.993	0.832	0.520	0.417
L2 - Z	Displacement	0.043	0.000	0.054	0.518	0.191	0.117	
Pelvis - X	Displacement	0.458	0.968	0.063	0.992	0.674	0.566	
Pelvis - Y	Displacement	0.084	0.842	0.319	0.986	0.716	0.400	0.362
Pelvis - Z	Displacement	0.042	0.000	0.090	0.514	0.201	0.122	
Shoulder [Left] - X	Displacement	0.170	0.253	0.197	0.960	0.470	0.320	
Shoulder [Left] - Y	Displacement	0.273	1.000	0.497	0.990	0.829	0.551	0.517
Shoulder [Left] - Z	Displacement	0.644	0.505	0.677	0.972	0.718	0.681	
Shoulder [Right] - X	Displacement	0.176	0.632	0.495	0.987	0.705	0.440	
Shoulder [Right] - Y	Displacement	0.148	1.000	0.463	0.998	0.820	0.484	0.488
Shoulder [Right] - Z	Displacement	0.240	1.000	0.544	0.981	0.842	0.541	

Other Results

Appendix B contains load, moment, and acceleration sensor time histories obtained from the simulations. Also included in Appendix B are subject support and restraint responses. Plots include force and moment time histories for the seat, knee bolster, and footrest load cells.

3 Discussion

Despite previous intensive efforts toward the development of HBMs, studies that evaluated the biofidelity of the HBM whole-body 3D kinematic response are rare. This is primarily because such detailed 3D occupant kinematic response data was only available recently with the use of the video-based optoelectronic stereo-photogrammetry methods like the method presented by Lessley et al., (2011). This study is the first attempt to assess the whole-body 3D kinematic response biofidelity of two human body FE models under near-side oblique frontal impact, a condition that was not used in the development of the models.

3.1 Model Bio-fidelity

The response of the THOR model was judged to reasonably close to the physical surrogate (Table 12). Similar kinematics, kinetics, and chest deflections were observed. Less forward and lateral excursions relative to the seat were observed, which potentially subject the models and the real dummy to different occupant posture and different impact locations. However, the ability to match chest deflections and internal instrumentation from the experiments suggest that these differences may not impact its ability to predict reasonable thoracic injury patterns.

Even though M50-OS and M50-O simulations were able to reproduce the predominant occupant motions observed in the PMHSs, both models also showed some response discrepancies compared to the PMHS responses. The discrepancies of the spine lateral displacement between the model and the PMHSs suggested potential differences of the trunk stiffness (combination of spine, ribcage and soft tissues/organs). Our results suggest that the neck muscles of the HBMs might be stiffer than the average response of a PMHS in this situation. Additional evaluation of the spine of M50-OS and M50-O at a hierarchical approach: from the component level (local) to the structure level (global) would help determine the correct model responses. Such component level assessment has the advantage of a more simplified and controlled loading condition compared to oblique impacts where boundary conditions uncertainty will affect model responses. Relevant evaluation of the HBM for the oblique crash condition could include evaluating the functional spine unit (FSU) level (Lopez-Valdes et al., 2014; Markolf, 1972; Panjabi et al., 1976) and whole lumbar spine level (Begeman et al., 1994; Demetropoulos et al., 1998).

3.2 Injury Assessment

The NHTSA THOR FE model is designed to allow output measurements similar to those that would be recorded by the instrumentation of the physical dummy so we assumed that comparing the instrumentation to THOR is the most appropriate solution for GS3.

M50-O was initially designed to predict fractures (rib, clavicle) using a deterministic method, inferred when a cluster of elements in the bone are eroded (deleted) at a predetermined strain threshold. However, in this study, we disabled element deletion for two reasons: (1) to allow comparison with M50-OS, and (2) to improve model stability. Consequently, rib fracture risk has been assessed using a strain-based injury risk function that could account for tolerance variations in the population. This method offers the advantage to account for age and other parameters without rerunning any additional simulation, but there is an argument about the effect of an accumulation of fractures that could result in a loss of structural stability that could affect the overall response (Forman et al., 2012). In this study, the model's ability to predict rib fracture in this situation was deemed satisfactory, with the limitation that we could not reproduce the severity of chest damage observed for two of the three subjects. However, the model's ability to predict cervical fracture was not deemed satisfactory since we could not reproduce the cervical damage observed for two of the three subjects.

Unlike its more detailed counterpart, the GHBMC M50-OS is not intended to predict crash induced injuries based on tissue-level criterion. The GHBMC M50-OS has virtual instrumentation (load cell, accelerometer, and deflection sensor), similar to an ATD, for injury risk assessment. The evaluation was performed through a quantitative evaluation of the virtual instrumentation data.

3.3 Potential Modeling Issues

The goal for model evaluation was also to identify any potential modeling issues (early termination, contact failure, element instability, etc.) that may affect the execution of the parametric study in Task 4. When encountered, we tried to correct the error using common model debugging techniques and approaches. When we were not able to correct an error, we documented the model limitations.

We identified and address the following issues:

1. In THOR FE, non-physical mesh distortion was observed in the shoulder pad due to belt integration, leading to early termination. We corrected this error by increasing the shoulder pad material stiffness and included this modification in the later simulations as this type of event in the parametric analysis is likely to occur.

2. In M50-O, early termination was observed in the pelvis with nodes shooting out-of-range in the flesh. Flesh remeshing was performed as well as decreasing the time step to limit the effect of mass scaling. This modification solved our stability issue, but significantly impacted the model performance and run time (+30%) that should not be a problem since M50-O was intended to be used in a limited number of cases in the parametric analysis.

4 Summary and Conclusions

In this task we successfully assessed the validity of the responses of the GHBMC M50-O, GHBMC M50-OS, and THOR FE models prior to their use in Task 4 and 5 by simulating each occupant model in the Gold Standard 3 (GS3) sled test condition. This sled test configuration is consistent with a frontal crash scenario with the seat oriented in-board, and it is a condition likely to be considered in Task 3. We replicated the GS3 test environment, performed simulations with the GHBMC and THOR models, and compared the results to the kinematic, kinetic, and injury responses observed in the PMHS or dummy tests via objective means (CORA).

We described the differences observed (with a discussion of their causes), potential effects on the evaluation of expected ADS-equipped vehicle seating conditions, and recommendations on how any biofidelity and/or injury prediction deficits could be addressed.

5 References

Acosta, S., Ash, J., Lessley, D. J., Shaw, C. G., Heltzel, S. B., & Crandall, J. R. (2016, September 14-16). *Comparison of whole body response in oblique and full frontal sled tests*. 2016 International Research Council on Biomechanics of Injury (IRCOBI) Conference, Malaga, Spain.

Begeman, P. C., Visarius, H., Nolte, L. P., & Prasad, P. (1998). Visocelastic shear responses of the cadaver and Hybrid III lumbar spine. *Stapp Car Crash Journal,38*:1-14.

Demetropoulos, C. K., Yang, K. H., Grimm, M. J., Khalil, T. B., & King, A. I. (1998). *Mechanical properties of the cadaveric and Hybrid III lumbar spines* (SAE Technical Paper 983160). Society of Automotive Engineers.

Forman, J. L., Kent, R. W., Mroz, K., Pipkorn, B., Bostrom, O., & Segui-Gomez, M. (2012) Predicting rib fracture risk with whole-body finite element models: development and preliminary evaluation of a probabilistic analytical framework. *Annals of Advances in Automotive Medicine, 56*:109-124.

Poulard, D., Subit, D., Donlon, J. P., & Kent, R. W. (2015). Development of a computational framework to adjust the pre-impact spine posture of a whole-body model based on cadaver tests data. *Journal of Biomechanics 48*:636-643.

Lopez-Valdes, F. J., Lau, S. H., Riley, P., & Kent, R. W. (2014, September 10-12). *Characterization of the in-vitro dynamic behavior of the human thoracic spine in flexion.* 2014 International Research Council on Biomechanics of Injury (IRCOBI) Conference, Berlin, Germany.

Markolf, K. L. (1972). Deformation of the thoracolumbar intervertebral joints in response to external loads: a biomechanical study using autopsy material. *Journal of Bone and Joint Surgery, American Volume, 54*:511-533.

Schwartz, D., Guleyupoglu, B., Koya, B., Stitzel, J. D., & Gayzik, F. S. (2015). Development of a computationally efficient full human body finite element model. *Traffic Injury Prevention, 16*:S49-S56.

Shaw, G., Parent, D., Purtsezov, S., Lessley, D., Crandall, J., Kent, R., Guillemot, H., Ridella, S. A., Takhounts, E., & Martin, P. (2009). Impact response of restrained PMHS in frontal sled tests: Skeletal deformation patterns under seat belt loading. *Stapp Car Crash Journal, 53*:1-48.

Nightingale, R. W., McElhaney, J. H., Richardson, W. J., & Myers, B. S. (1996). Dynamic responses of the head and cervical spine to axial impact loading. *Journal of Biomechanics, 29*(3):307-18.

Nightingale, R. W., McElhaney, J. H., Camacho, D. L., Kleinberger, M., Winkelstein, B. A., & Myers, B. S. (1997). The dynamic response of the cervical spine: Buckling, end conditions, and tolerance in compressive impacts. *Stapp Car Crash Journal, 74*:451-471.

Panjabi, M. M., Brand, R. A., & White, A. A. (1976). Three-dimensional flexibility and stiffness properties of the human thoracic spine. *Journal of Biomechanics, 9*(4):185-92.

Appendix A: Sensor Data Plots – GHBMC M50-OS and GHBMC M50-O

Upper Shoulder Belt Load

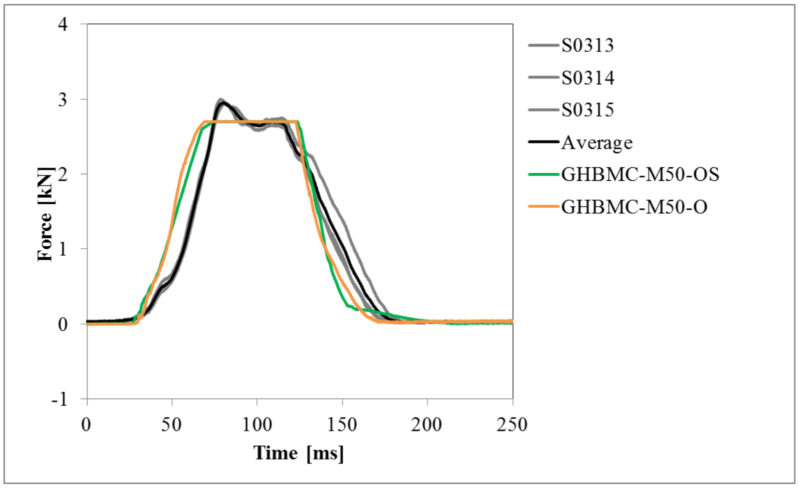

Lower Shoulder Belt Load

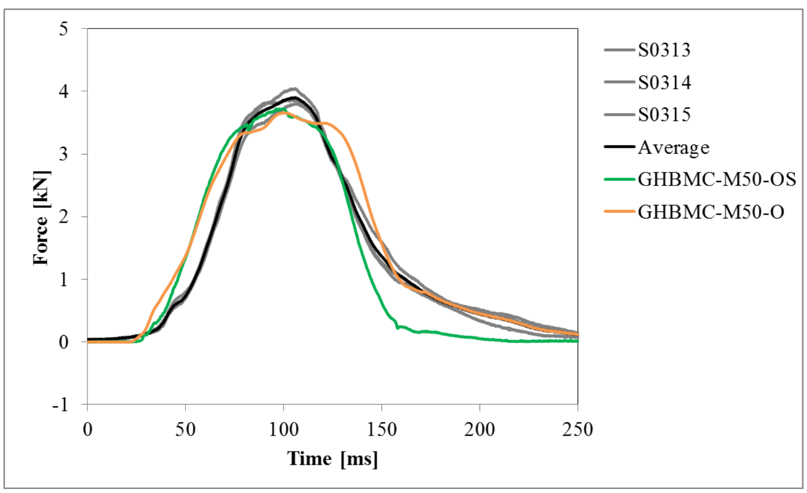

Lap Belt Load

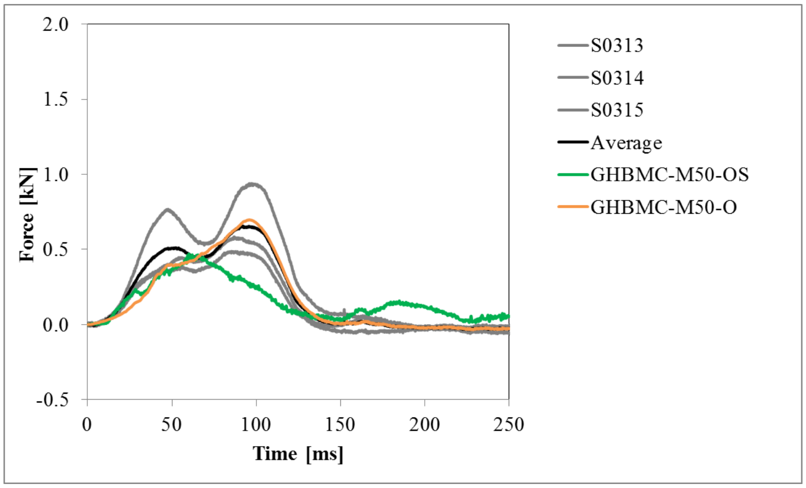

Seat Load (resultant)

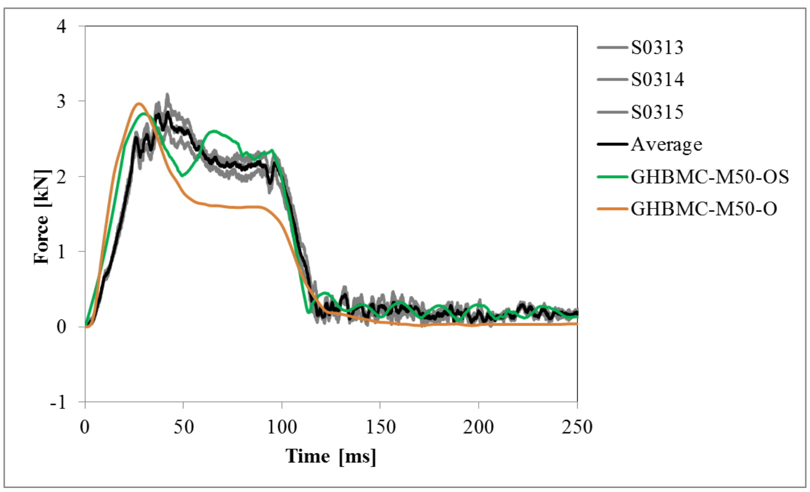

Footrest (resultant)

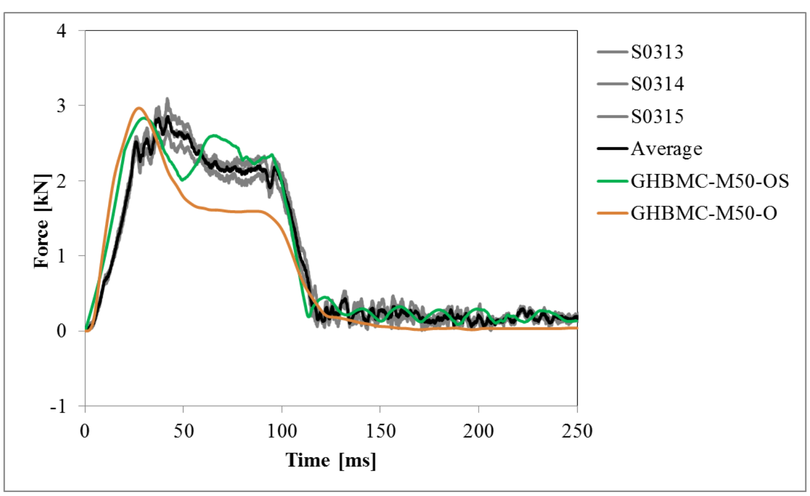

Head – X

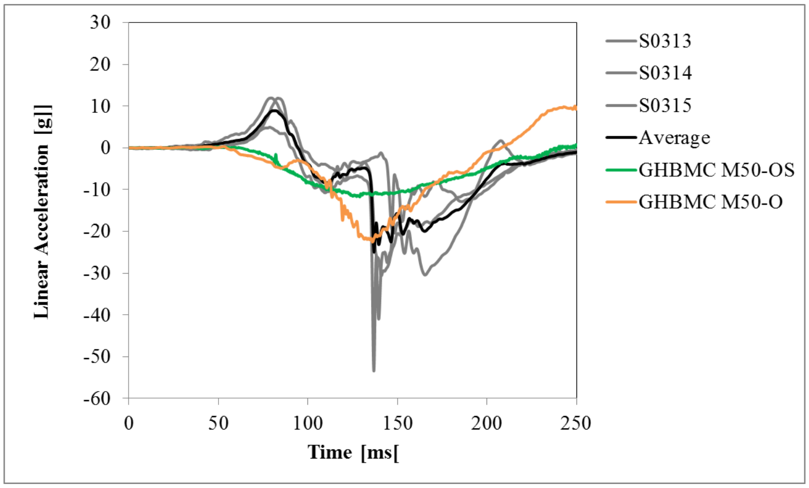

Head – Y

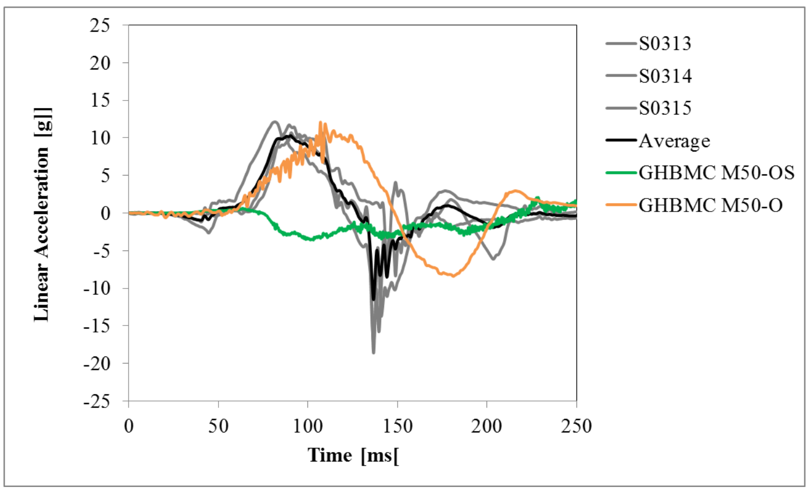

Head – Z

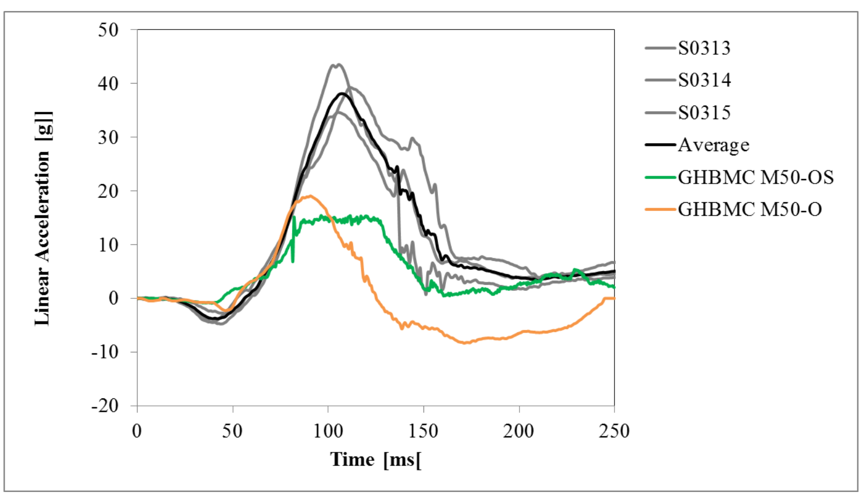

T1 –X

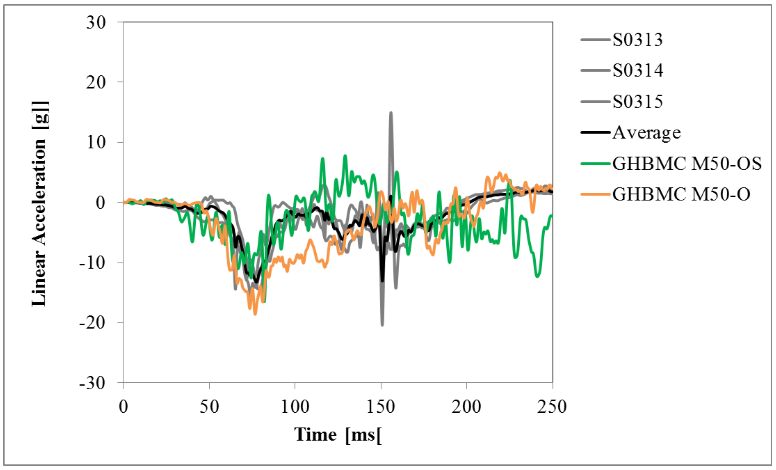
30
20
10
0
-10
-20
-30
Linear Acceleration [g]]
0
50
100
150
200
250
Time [ms[
S0313
S0314
S0315
Average
GHBMC M50-OS
GHBMC M50-O

T1 – Y

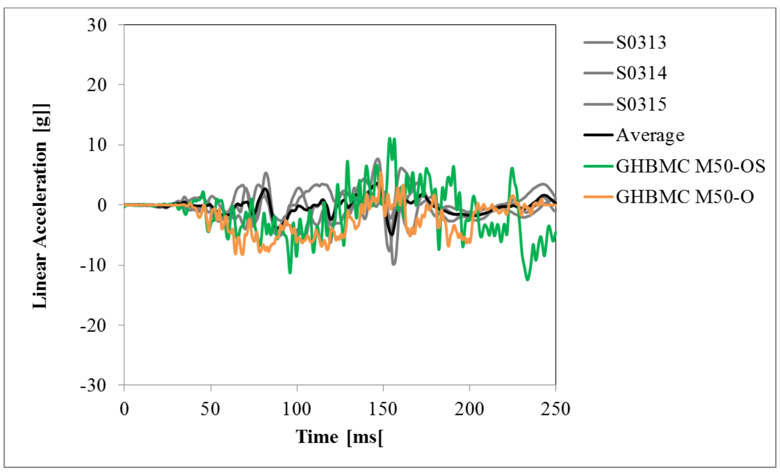
30
20
10
0
-10
-20
-30
Linear Acceleration [g]]
0
50
100
150
200
250
Time [ms[
S0313
S0314
S0315
Average
GHBMC M50-OS
GHBMC M50-O

T1 – Z

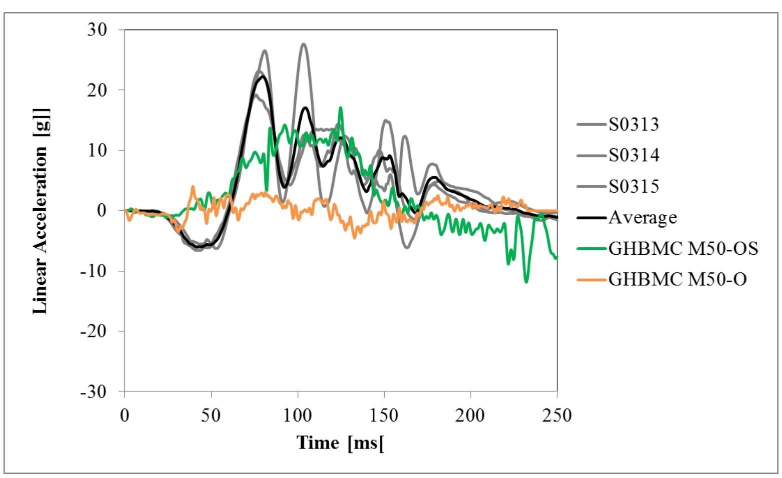
30
20
10
0
-10
-20
-30
Linear Acceleration [g]]
0
50
100
150
200
250
Time [ms[
S0313
S0314
S0315
Average
GHBMC M50-OS
GHBMC M50-O

T8 - X

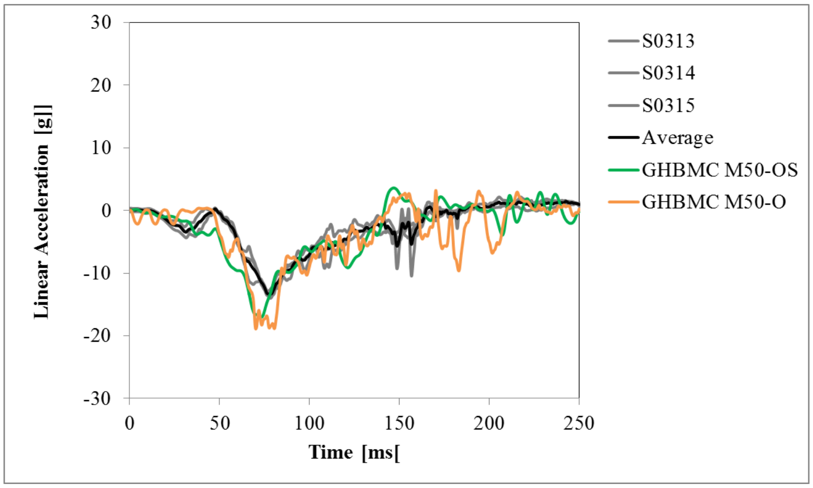

30
20
10
0
-10
-20
-30
0
50
100
150
200
250
Linear Acceleration [g]]
Time [ms[
S0313
S0314
S0315
Average
GHBMC M50-OS
GHBMC M50-O

T8 – Y

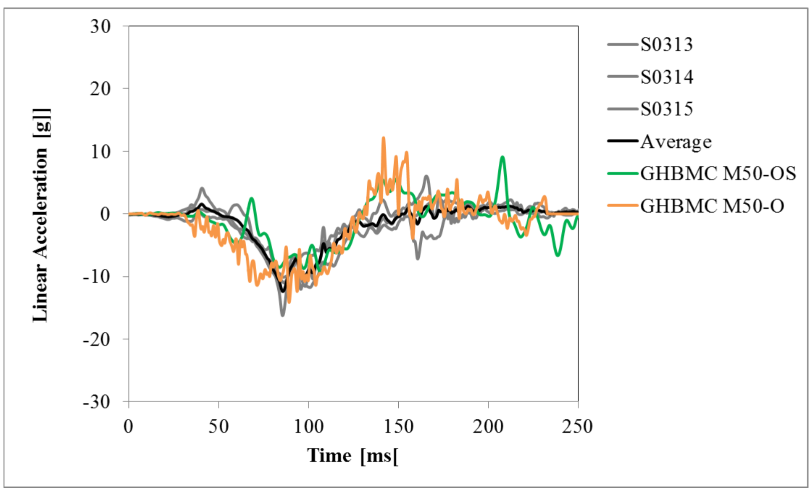

30
20
10
0
-10
-20
-30
0
50
100
150
200
250
Linear Acceleration [g]]
Time [ms[
S0313
S0314
S0315
Average
GHBMC M50-OS
GHBMC M50-O

T8 – Z

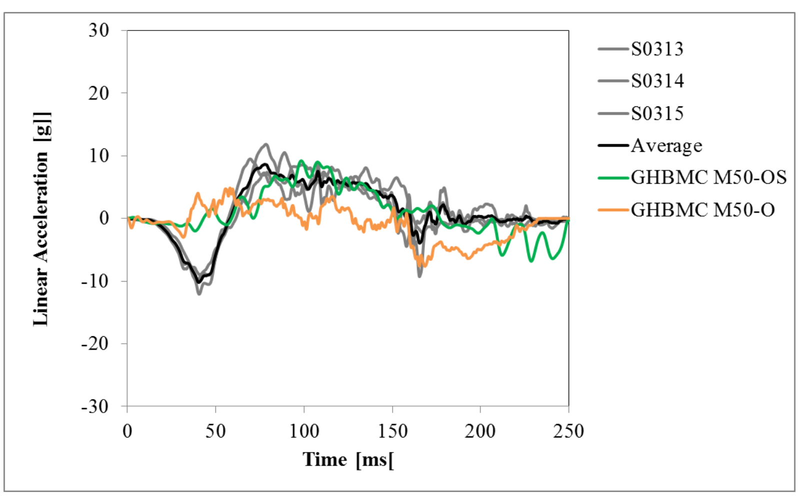

30
20
10
0
-10
-20
-30
0
50
100
150
200
250
Linear Acceleration [g]]
Time [ms[
S0313
S0314
S0315
Average
GHBMC M50-OS
GHBMC M50-O

Pelvis – X

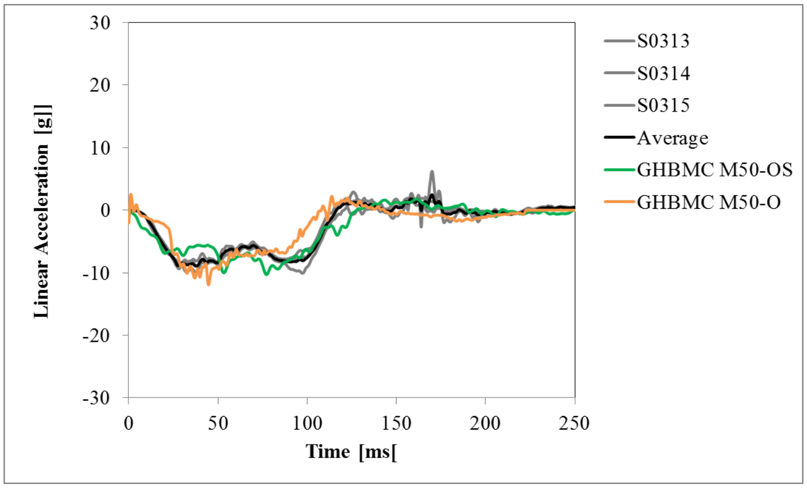

Pelvis – Y

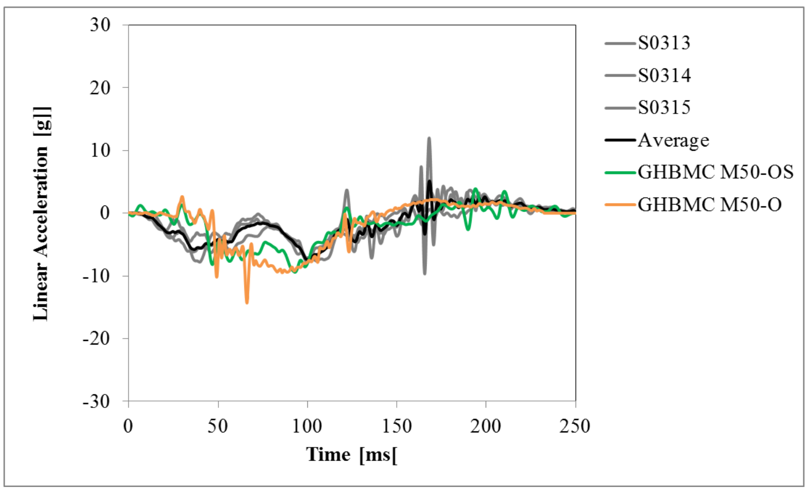

Pelvis – Z

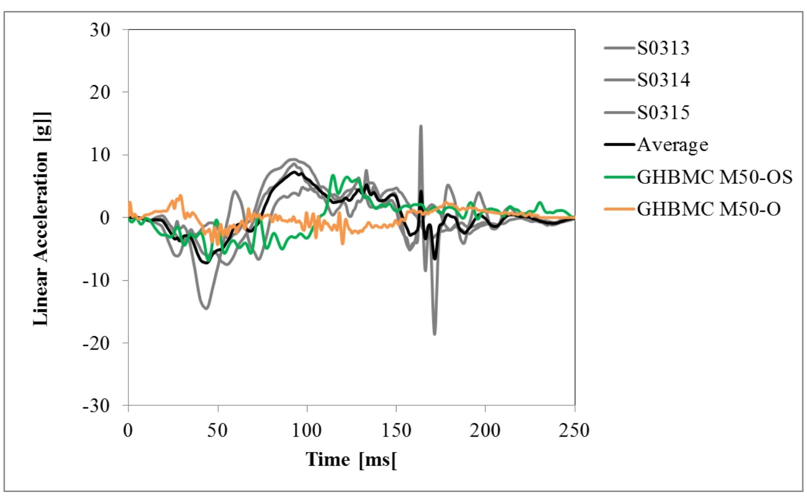

Appendix B: Sensor Data Plots – THOR FE

Upper Shoulder Belt Load

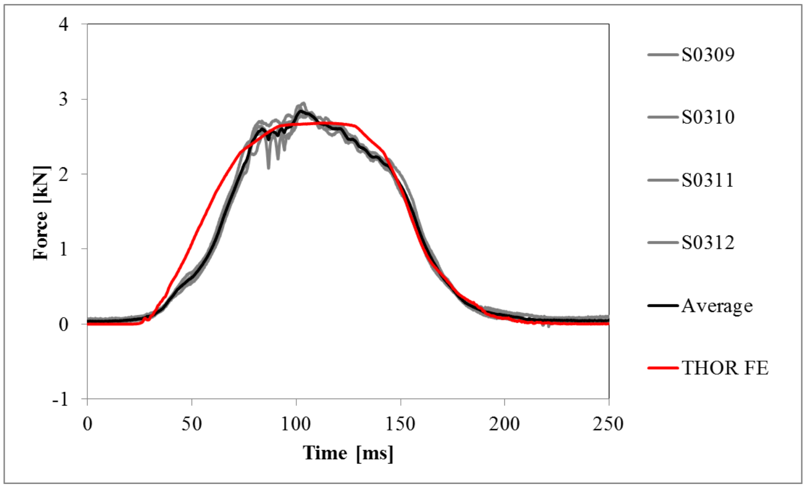

Lower Shoulder Belt Load

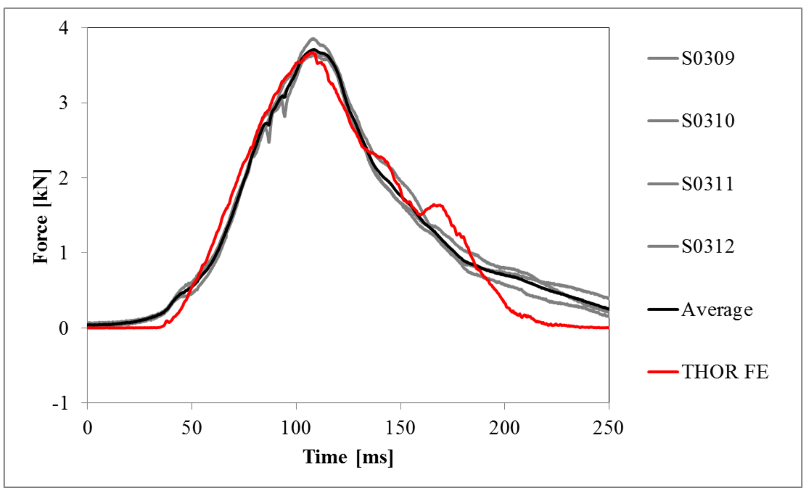

Lap Belt Load

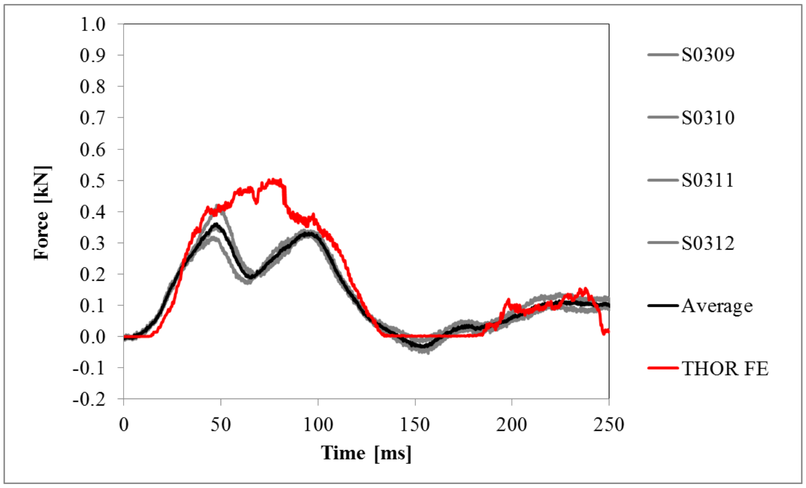

Seat Load (resultant)

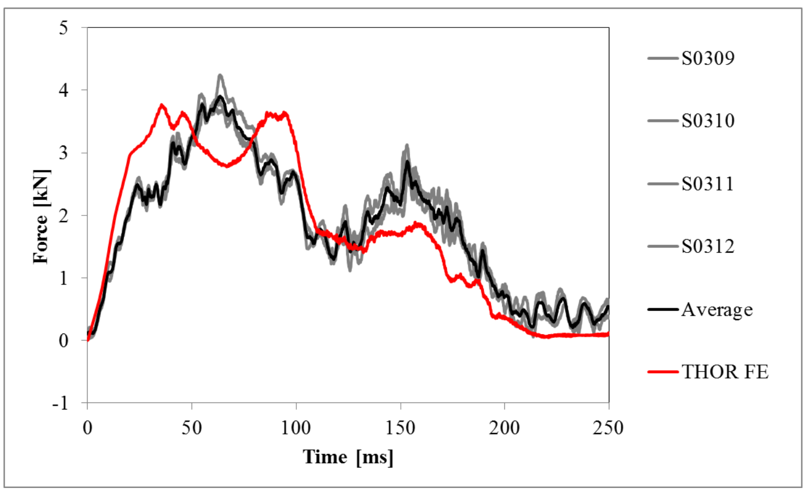

Kneebolster [Left] (resultant)

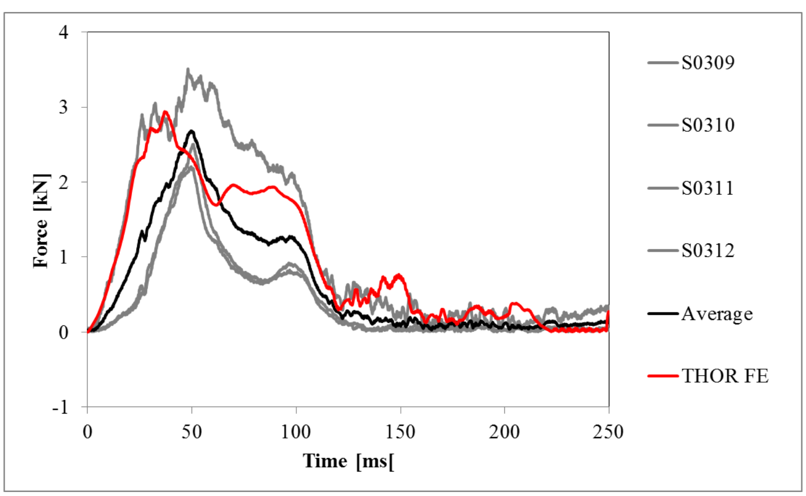

Kneebolster [Right] (resultant)

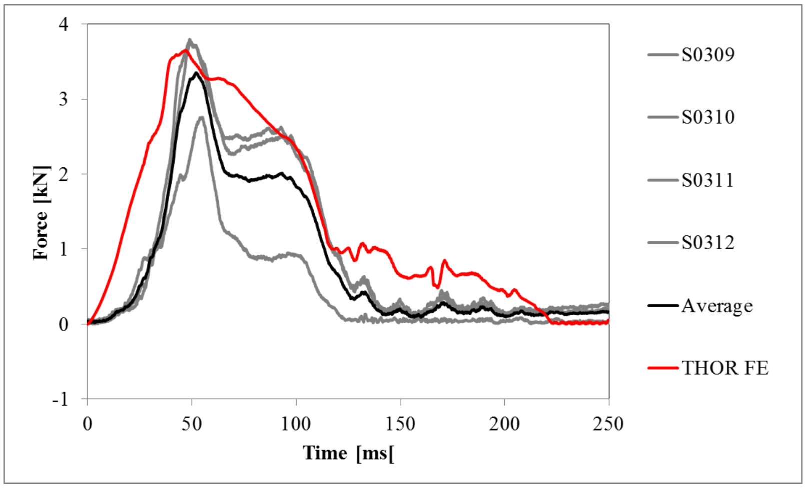

Footrest (resultant)

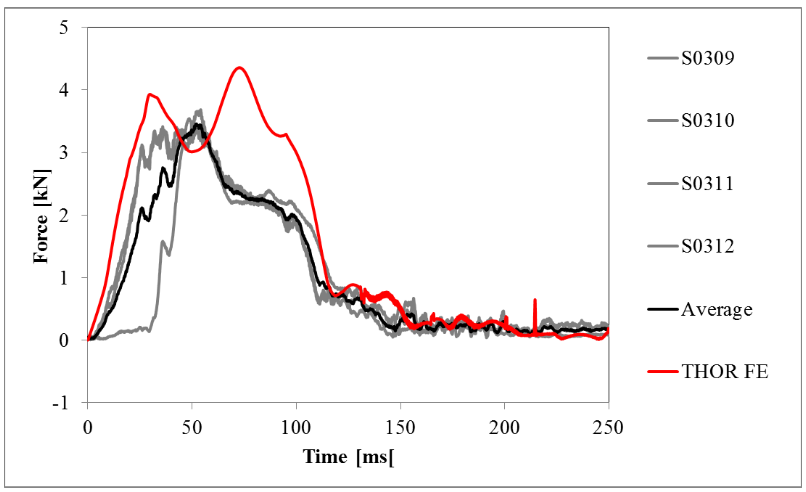

Head – X

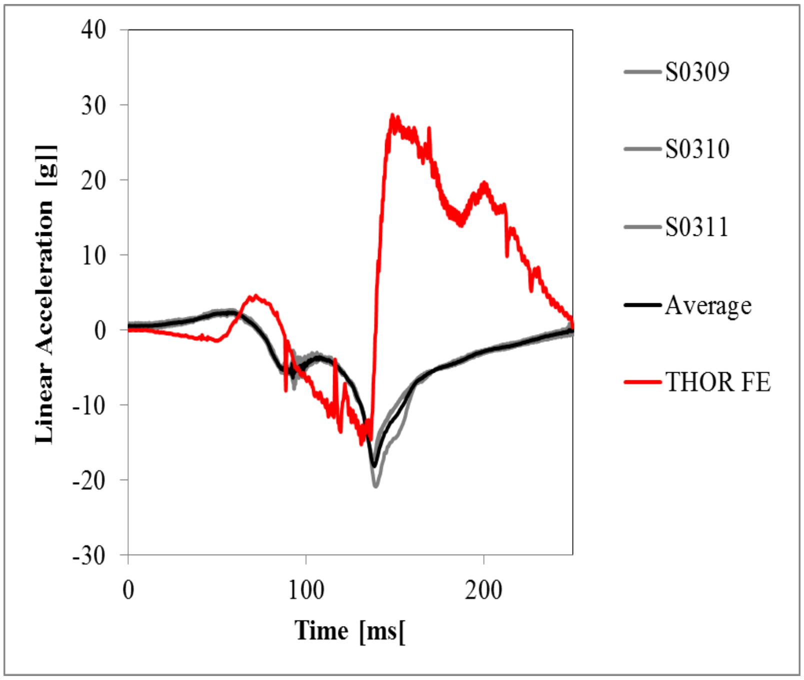

40
30
20
10
0
-10
-20
-30
Linear Acceleration [g]]
0
100
200
Time [ms[
S0309
S0310
S0311
Average
THOR FE

Head – Y

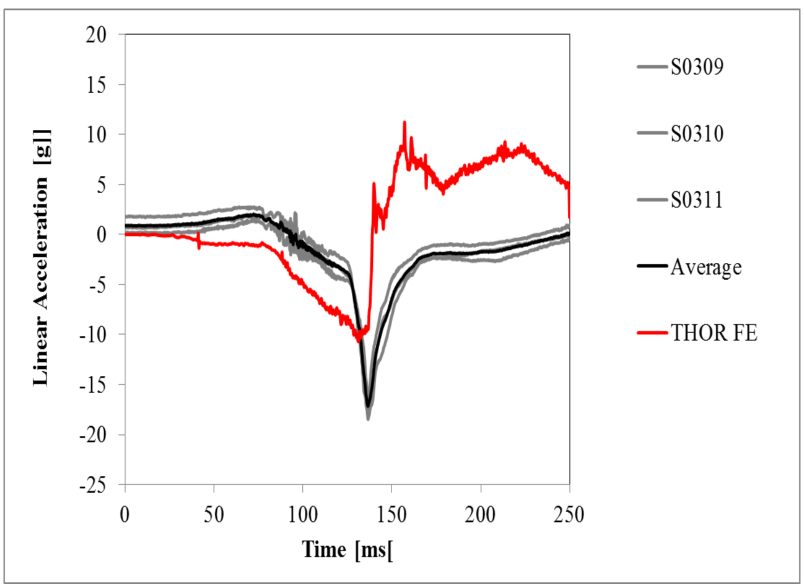

20
15
10
5
0
-5
-10
-15
-20
-25
Linear Acceleration [g]]
0
50
100
150
200
250
Time [ms[
S0309
S0310
S0311
Average
THOR FE

Head – Z

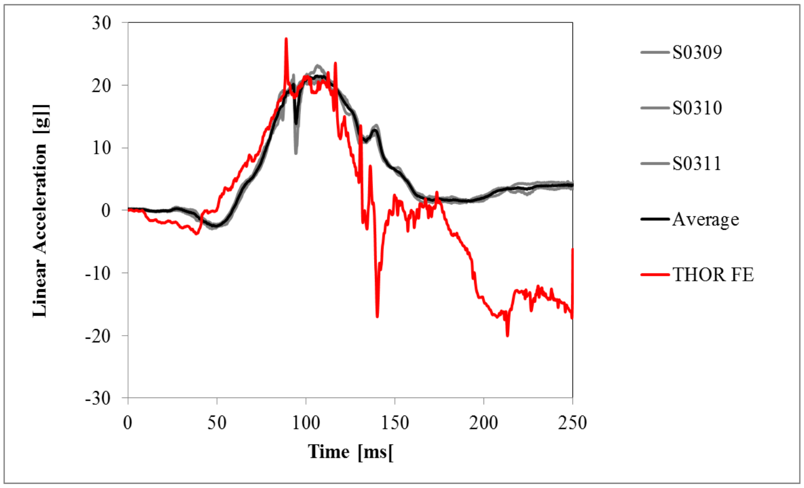

T1 – X

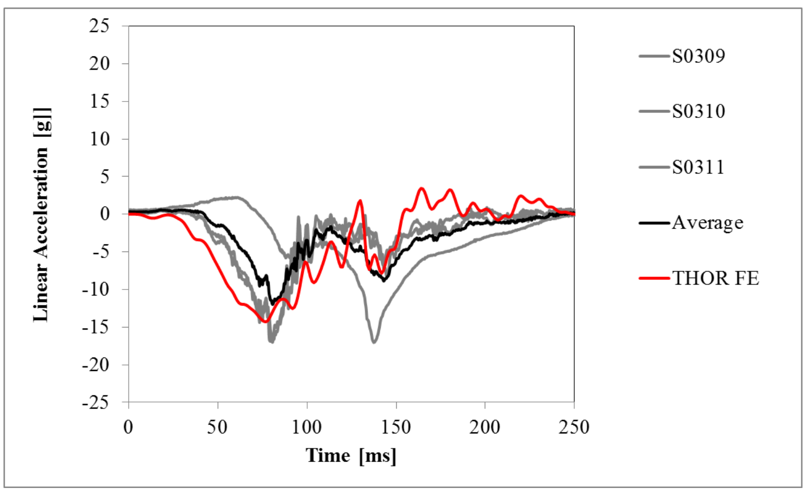

T1 – Y

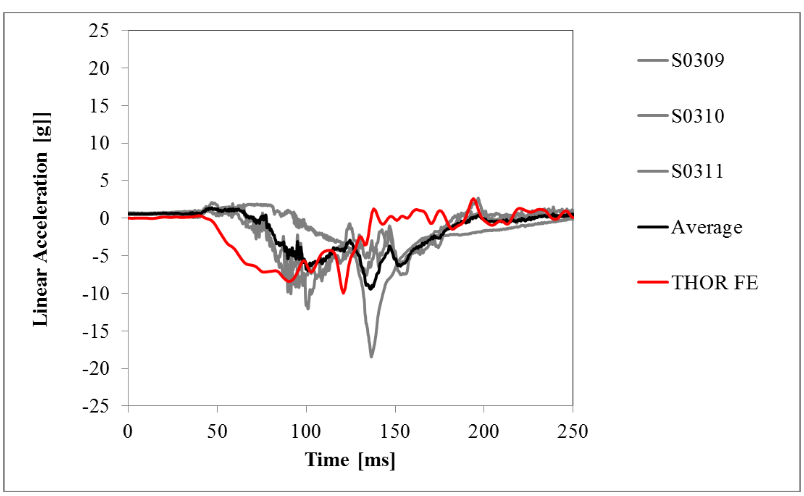

T1 – Z

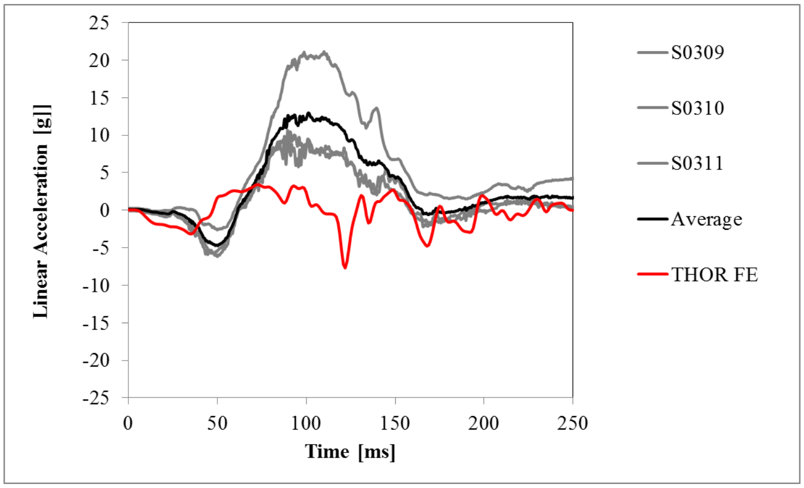
25
20
15
10
5
0
-5
-10
-15
-20
-25
0
50
100
150
200
250
Time [ms]
Linear Acceleration [g]]
S0309
S0310
S0311
Average
THOR FE

Pelvis – X

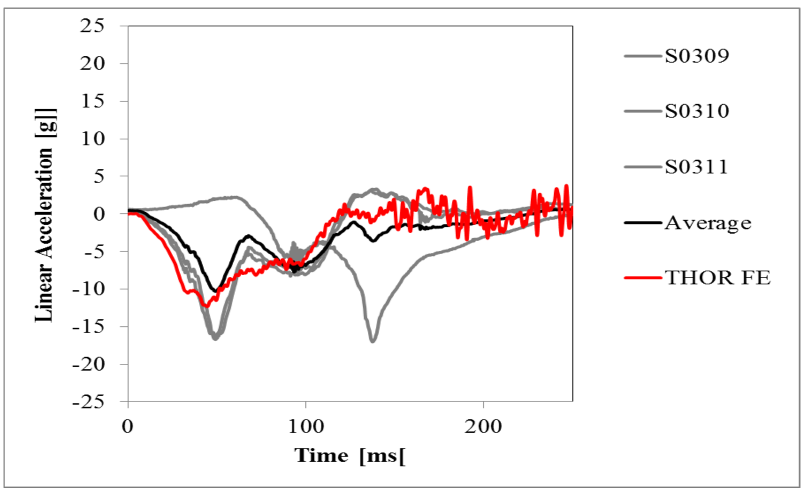
25
20
15
10
5
0
-5
-10
-15
-20
-25
0
100
200
Time [ms[
Linear Acceleration [g]]
S0309
S0310
S0311
Average
THOR FE

Pelvis – Y

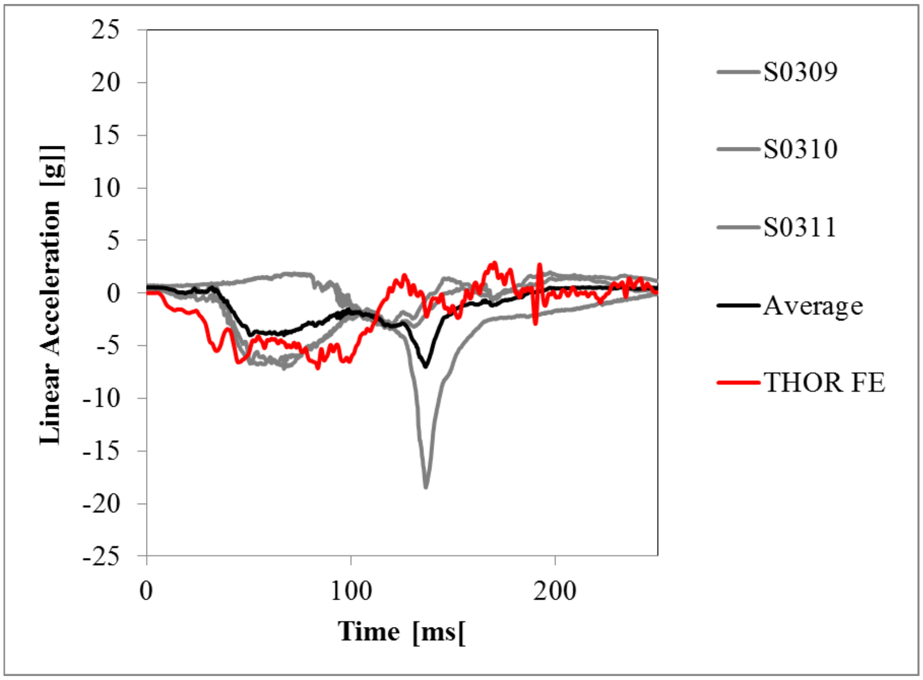

Pelvis – Z

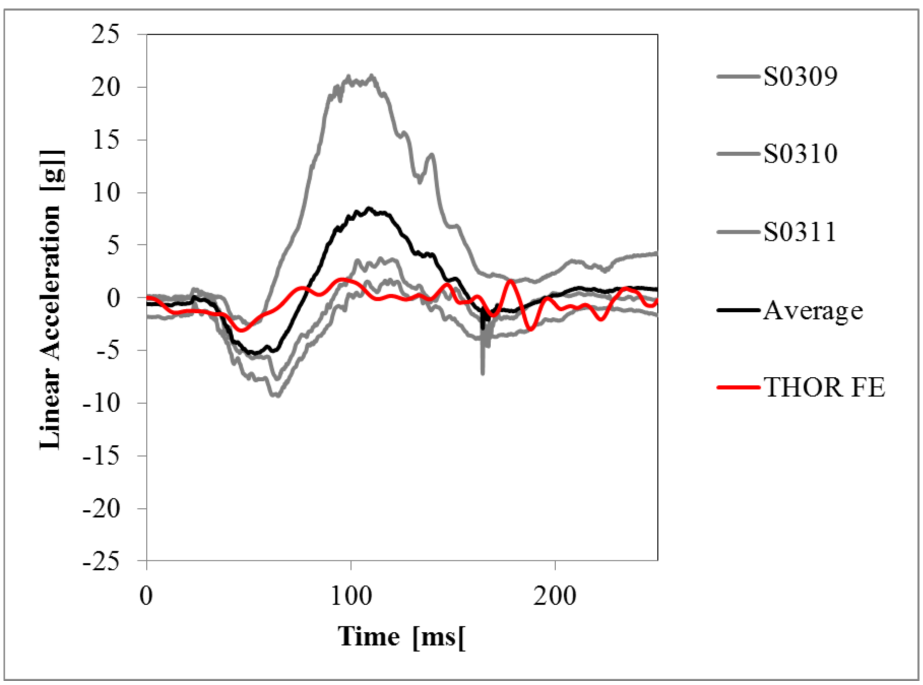

DOT HS 812 905
July 2020

U.S. Department
of Transportation

National Highway
Traffic Safety
Administration

NHTSA

14619-070820-v6